

# Assessment of Short-medium Term Intervention Effects Using CAE-SAR-Lisflood in Post-earthquake Mountainous Area

Di Wang<sup>1,2,3</sup>, Ming Wang<sup>1</sup>, Kai Liu<sup>1</sup>, [Jun Xie<sup>1</sup>](#)

<sup>1</sup>School of National Safety and Emergency Management, Beijing Normal University, Beijing, China.

<sup>2</sup>Academy of Disaster Reduction and Emergency Management, Beijing Normal University, Beijing, China.

<sup>3</sup>Faculty of Geographical Science, Beijing Normal University, Beijing, China.

Correspondence to: Ming Wang ([wangming@bnu.edu.cn](mailto:wangming@bnu.edu.cn))

**Abstract.** The 2008 Wenchuan earthquake triggered local geomorphic changes rapidly ~~and gradually~~, producing abundant ~~materials~~material through ~~external~~exogenic processes. The substantial ~~materials~~material dynamics increased the risks of ~~geo-~~morphic-geo-hazards (flash floods, landslides, and debris flows) induced by extreme precipitation in the area. Intervention measures such as dams, levees, and vegetation revetments have been constructed in specified sites to reduce sediment transport, thus mitigating the risk of ensuing geo-hazards.

This study ~~concentrated~~focused on assessing intervention effects incorporated with various facilities on post-earthquake fragile mountains in the short-medium term. Taking the Xingping valley as an example, we used the CAESAR-Lisflood, a two-dimensional landscape evolution model, to simulate three scenarios: unprotected landscapes, present protected landscapes, and enhanced protected landscapes between 2011 and 2013. We ~~compared the geomorphic changes and~~ defined two indicators to assess the intervention effects of the three scenarios by comparing the geomorphic changes and sediment yield.

The results showed that the mitigation facilities were effective, especially engineering efforts cooperating with vegetation revetments in the upstream area. The ~~distributions~~spatial patterns of erosion and deposition changed considerably ~~by~~caused of the intervention measures. Additionally, the effectiveness of each intervention scenario showed a gradual decline caused directly by the reduction of the reservoir capacity. ~~Besides, the~~The enhanced scenario functioned better than the present one, with a smaller ~~descent slope~~downward trend. The simulation ~~methods~~results assessed the ability and effectiveness of cooperated control measures and could support optimum mitigation strategies.

## 1 Introduction

Strong earthquakes trigger co-seismic landslides and crack the mountains discontinuously, increasing weak structural planes (Huang, 2009) by weathering and erosion. Consequently, the source ~~materials~~material produced from co-seismic landslides and attendant mass failure caused by the weak slope increase in mountainous regions and modify mountain landscapes by various surface processes for days, years, and millennia (Fan et al., 2020). The 2008 Wenchuan ~~2008~~-Ms= 8.0 (the surface-wave magnitude, which is the logarithm of the maximum amplitude of ground motion for surface waves with a wave period of 20 seconds) earthquake ~~influence~~has been influencing towns and other infrastructure in the affected area. Many studies have mapped the landslides triggered by the devastating earthquake. Gorum et al. (2011) performed an extensive landslide interpretation using a large set of high-resolution optical images and mapped nearly 60000 individual landslides, which are no less than ~~600m<sup>2</sup>~~600 m<sup>2</sup>. Xu et al. (2014) delineated 197481 landslides formed by polygons, centroids, and top points compiled from visual image interpretation. To estimate the threat of loose ~~materials~~material in subsequent sediment disasters caused by landslides, some research attempt to measure the volume of deposited ~~materials~~material based on field survey and assumptions. Huang and Fan (2013) estimated 400 million m<sup>3</sup> of ~~materials~~material deposited in the heavy-affected areas by assuming that the ~~materials~~material deposited on steep slopes with angles larger than 30° and a catchment area of more-~~extensive~~ than 0.1 km<sup>2</sup>. An approximate 2793 million m<sup>3</sup> of sediment was calculated by Chen et al. (2009) using different deposited depth settings

39 in different buffer zones of the Longmenshan central fault. In summary, a tremendous number of loose ~~materials are suspended~~  
40 ~~material accumulated~~ on the gullies and ~~hill slopes and hillslopes~~, ready to be eroded and transported away over a long time.  
41 ~~Therefore~~ As a result, the mitigation ~~is still in the long run~~ in the Wenchuan quake-stricken area is still in the long run.  
42 Structural mitigation measures have been developed in the affected areas regarding the site conditions and technical and eco-  
43 nomic feasibilities. For example, ~~Ecological~~ ecological mitigation such as vegetation revetments was conducted to ~~stabilize~~ stabilize  
44 the source area in hillslopes (Cui and Lin, 2013; Forbes and Broadhead, 2013; Stokes et al., 2014), and check dams were  
45 used widely to intercept upriver sediment (Yang et al., 2021; Marchi et al., 2019) (Yang et al., 2021; Marchi et al., 2019). Lateral  
46 walls and levees were the longitude structures (Marchi et al., 2019) to protect the infrastructures in mountain watersheds with  
47 higher sediment supply to the main streams.

48 Although comprehensive mitigation measures were performed in potentially dangerous sites, disasters still occurred owing to  
49 rough terrain, vague source ~~materials~~ material, intensive precipitation, and relatively low-cost mitigating measures (Yu et al.,  
50 2010; Cui et al., 2013). Therefore, understanding the effectiveness of intervention measures is crucial for mitigation strategies.  
51 ~~More~~ Some studies mainly focus on establishing post-evaluation effectiveness index systems that are not supported by suffi-  
52 cient practices (Zhang and Liang, 2005; Wang et al., 2015). ~~Other research on long term on site measurement required more~~  
53 ~~energy and financing and compared~~ Some researchers compare the changes before and after the intervention measures recorded  
54 by the long-term on-site measurement, which face the challenges to the investment of much time, energy and financing (Zhou  
55 et al., 2012; Chen et al., 2013). Recent research compares the disaster characteristics before and after the ~~intervention~~ mitigation  
56 actions, which are quickly obtained from the numerical simulation (Cong et al., 2019; He et al., 2022). Nevertheless, ~~the~~ these  
57 disaster characteristics express the process ignoring the long-time effects on the geomorphic changes (longer than the duration  
58 of a single event). Therefore, the short-medium term (from the duration to decades) and spatial geomorphic changes quickly  
59 obtained from the simulation will provide more details to interpret engineering measures in notable locations, even in those  
60 inaccessible to humans.

61 ~~The open access 2-D landscape evolution model~~ CAESAR-Lisflood (C-L), which is based on the Cellular Automata (CA)  
62 framework (Coulthard et al., 2013), ~~which~~ has powerful spatial modelling and computing capabilities to simulate complex  
63 dynamic systems (~~Batty and Xie, 1997; Couclelis, 1997; Coulthard et al., 2002~~) (Batty and Xie, 1997; Couclelis, 1997;  
64 Coulthard et al., 2002). The model enables the study of many earth system interactions with under different geo-environmental  
65 forces. Representation of deposition and erosion within C-L is used widely in rehabilitation planning and soil erosion  
66 predictions from a post-mining landform (Saynor et al., 2019; Hancock et al., 2017; J.B.C. Lowry et al., 2019; Thomson and  
67 Chandler, 2019; Slingerland et al., 2019) (Saynor et al., 2019; Hancock et al., 2017; J.B.C. Lowry et al., 2019; Thomson and  
68 Chandler, 2019; Slingerland et al., 2019) and channel evolution and sedimentary budget with dam settings (Poeppl et al., 2019;  
69 Gioia and Schiattarella, 2020; Ramirez et al., 2020, 2022) (Poeppl et al., 2019; Gioia and Schiattarella, 2020; Ramirez et al.,  
70 2020, 2022). In addition, there ~~have been~~ were a series of studies in the mountainous area involving secondary geo-hazard  
71 driving factors (Li et al., 2018; Wang et al., 2014b) and vegetation recovery (Zhang et al., 2018). Li et al. (2020) and Xie et al.  
72 (2018) have used C-L with different rainfall scenarios or future climate change to interpret the landscape evolution after the  
73 Wenchuan earthquake. The methods and parameter values used in the above research helped to promote the application in  
74 other study areas.

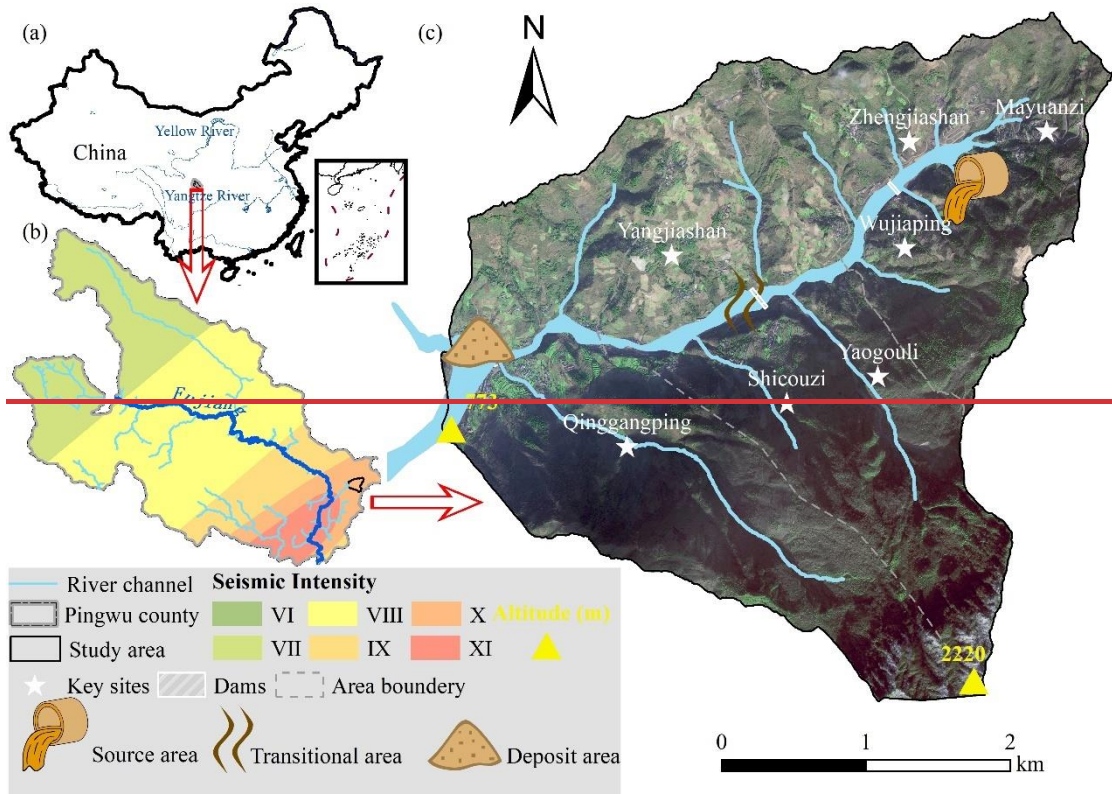
75 In this study, the hourly rainfall data of three years was generated by downscaling from daily to capture the extreme event.  
76 Based on the input data, we simulated and compared the geomorphic changes and sediment ~~output~~ yield in three scenarios that  
77 varied in mitigation compositions and intensities in a catchment. The objectives are to 1) assess the effectiveness of a set of  
78 mitigation facilities in ~~reducing~~ to reduce sediment transport, 2) analyse the role of each facility in ~~on~~ geomorphic changes, and  
79 3) determine vegetation influence on catchment erosion.

80 **2 Study area**

81 **2.1 Regional characteristics**

82 The study area was Xingping valley in the northeastern Sichuan province, a left branch of the Shikan river (a tributary of the  
83 Fu River) (Figure 1). There are nearly two hundred households scattered among more than five villages in the catchment. The  
84 topography of the catchment is rugged, with an elevation between 800 and 3036 m and an area of approximately 14 km<sup>2</sup>. The  
85 catchment ~~shape looks like a "leaf" with a nearly U-shaped main ditch~~ is characterised by a high longitudinal gradient (~ 120%)  
86 and more than ten small V-shaped branch gullies. The length from northeast to southwest is 5770 m, the other direction per-  
87 pendicular to which is 4150 m. A humid temperate climate with a mean annual temperature of 14.7°C characterises the region.  
88 The mean annual precipitation is 807.6 mm, ~~with maxima daily rainfall mainly concentrated~~ between May and September. The  
89 steep terrain and short-term heavy rainfall make an ephemeral stream in this area.

90 The local basement rocks are mainly metamorphic sandstones, sandy slate, crystalline limestone, and phyllite of Triassic  
91 Xikang Group (T<sub>3xk</sub>) and Silurian Maoxian Group (S<sub>mx</sub>), which ~~are easily worn away by~~ quickly ~~induce a large amount of loose~~  
92 ~~solid material after~~ weathering ~~of~~ in a static process, ~~after disturbed in a strong earthquake~~. Consequently, the Wenchuan earth-  
93 quake ~~that, with a Modified Mercalli Intensity scale of X,~~ made this area one of the most severely affected locations ~~with a~~  
94 ~~Modified Mercalli Intensity scale of X~~ (Wang et al., 2014a) ~~and~~ produced 10<sup>6</sup> m<sup>3</sup> ~~loose material~~ by triggering landslides ~~fro-~~  
95 ~~and subsequent weathering in~~ Mayuanzi, Zhengjiashan, and Wujiaping (Figure 1)(Guo et al., 2018).



96

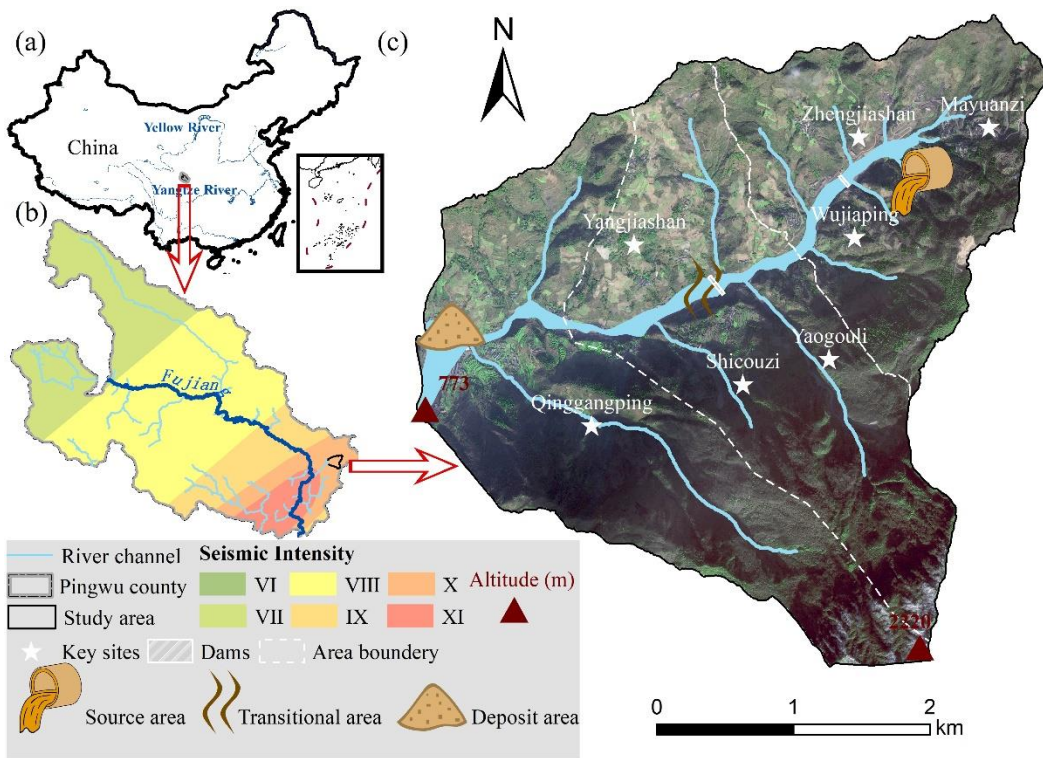


Figure 1: The location overview of the study area. (a) Location within China of study area; (b) Location within the seismic intensity ranges map of the Wenchuan earthquake and within the Pingwu county; (c) The schematic image of the study area.

## 2.2 Historical hazards and intervention measures

Six group debris flow-flash flood disaster chains were have been found in Xingping valley decades over a decade after the earthquake. Based on the published work of SKLGP (State Key Laboratory of Geohazard Prevention and Geoenvironment Protection) and the local states' geological survey before 2018 and our biannual field surveys since 2012, we catalogued the time of occurrence, total rainfall of each event, corresponding disaster details in (Table S1-). The massive sediment was transported quickly after the devastating quake in 2008 and 2009. The, and the extreme rainfall in 2013 and 2018 induced triggered prosperous loose materials material deposited in the channel. Considering the landslide processes, we divided the study area into three regions: source area, transitional area, and deposit area (the greywhite dashed lines in Figure 1c), which meant means the loose solid materials material would be easily transported from the source area to the deposit one through the transitional zone.

An engineering control project was completed constructed to intercept the upriver materials material in October 2010. The project included two check dams, one in the upper source area and the other in the transitional zone (Feng et al., 2017) (Figure 1c). The upper dam has a storage capacity of  $5.78 \times 10^4 \text{ m}^3$  and a height of 10.0 m. The transitional area dam has a storage capacity of  $7.2 \times 10^4 \text{ m}^3$  and a height of 9.0 m. With the reservoirs gradually filling with deposits, the first dredging work was subsequently done in 2013. Nearly three years later, the storage capacity behind the upper dam remained at 50% in 2016, while the transitional area dam cannot can no longer retain sediment.

## 3 Materials and Methods

In this study, we examined the intervention effectiveness through the morphological response and sediment yield in the Xingping valley, which was simulated using the C-L model. The research entailed four main steps: 1) setting three scenarios varied with different intervention compositions, 2) preprocessing the model input data, including three groups of DEMs, the rainfall data, and m values value of the C-L, 3) calibration of the hydrological component, and 4) simulating a three year of the landscape changes and analysing the intervention effectiveness in 2011-2013.

### 122 3.1 Scenarios settings

123 The abundant source ~~materials~~material triggered by landslides should be controlled to prevent the threat of disasters down-  
124 stream. Therefore, we designed three scenarios by incorporating engineering and biological measures referenced to current  
125 facilities to assess the effectiveness of intervention measures. Scenario UP: Unprotected landscapes meant the sediments would  
126 transport without anthropogenic intervention. Scenario PP: Present protected landscapes implied that only the present two  
127 check dams trapped deposits in 2011-2013 without dredging work over the period (see section 2.2). Scenario EP: Enhanced  
128 protected landscapes emphasised the plus vegetation revetments in the source area and levees in the deposit area based on the  
129 two check dams in Scenario PP.

130 Figure 1c shows the locations of the existing two check dams in both Scenario PP and Scenario EP. We determined the place-  
131 ments of additional facilities in Scenario EP according to the field survey, which demonstrated that the continuous supply of  
132 sediments was mainly from the source area. Therefore, the vegetation revetments like ~~tree~~tree planting would be carried out  
133 upriver for their ability in upstream to prevent erosion by stabilising topsoil and enhancing the soil's infiltration capacity with  
134 its roots (Lan et al., 2020).

135 Considering ~~that~~ the damages caused by flash-flood gushed in and damaged to the residential area downriver downstream, the  
136 levees (see Fig. 2S1 and Section 3.2.2), ~~the levees~~ are artificial barriers to protect agricultural land and buildings, which  
137 helped to prevent ~~the mixture of~~ water and sediment from overflowing and flooding surrounding areas. ~~We simulated and~~  
138 ~~compared the three types of situations described above.~~ Table 1 shows the scenario descriptions, initial model conditions and  
139 input rainfall series. The details about model input data are introduced below.

140 Table 1: Scenarios setting

<u>Scenario</u>	<u>Descriptions</u>	<u>Period</u>	<u>DEM (10m)</u>	<u>Rainfall data</u>
<u>UP</u>	<u>no anthropogenic intervention</u>		<u>UP DEM</u> <u>UP bedDEM</u>	<u>downscaled hourly pre-</u> <u>cipitation in the period</u>
<u>PP</u>	<u>the present two check dams upstream</u> <u>without dredging work</u> <u>additional vegetation revetments in the</u>	<u>2011-2013</u> <u>(3 years)</u>	<u>PP DEM</u> <u>PP bedDEM</u>	<u>(lumped)</u>
<u>EP</u>	<u>source area and levees in the deposit area</u> <u>based on Scenario PP</u>		<u>EP DEM</u> <u>EP bedDEM</u>	<u>downscaled hourly pre-</u> <u>cipitation in the period</u> <u>(spilt)</u>

### 142 3.2 CAESAR-Lisflood

143 The C-L ~~model~~ integrated the Lisflood-FP 2D hydrodynamic flow model (Bates et al., 2010) with the CAESAR landscape  
144 evolution model (LEM) (~~Coulthard et al., 2002; Van De Wiel et al., 2007~~)(Coulthard et al., 2002; Van De Wiel et al., 2007),  
145 which is ~~entirely~~ described in detail by Coulthard et al. (2013). ~~We used the~~ The catchment mode ~~that required~~ of C-L was  
146 applied in this study, within which the surface digital elevation model (DEM), the bedrock DEM, the grain size distribution,  
147 and a rainfall time series are required to simulate the sediment transport and ~~geomorphological~~geomorphic changes ~~in this~~  
148 ~~study. The~~ There are four primary modules ~~operate within C-L operated~~ as follows:

- 149 (1) a hydrological module generates surface runoff from rainfall ~~rates~~input using an adaption of TOPMODEL (Topography  
150 based hydrological model) (Beven and Kirkby, 1979),
- 151 (2) a hydrodynamic flow routing module based on the Lisflood-FP method (Bates et al., 2010) calculates the flow depths and  
152 velocities,
- 153 (3) an erosion and deposition module uses hydrodynamic results to drive fluvial erosion by either the Einstein (1950) or the  
154 Wilcock et al. (2003) equation applied to each sediment fraction over nine different grain sizes,
- 155 (4) and a slope model ~~eliminates materials~~moves material from the ~~slope~~hillslope to the fluvial system by considering both the  
156 mass movement when a critical slope threshold is exceeded, and soil creep processes whereby sediment flux is linearly pro-  
157 portional to surface slope.

The C-L model updates ~~variables~~variable values stored in square ~~gridded~~grid cells at intervals, such as DEM, grain size and proportion data, water depth, and velocity. For three scenarios, the initial conditions, such as DEMs and bedrock DEMs, the rainfall data, and the m values were ~~reprocessed~~preprocessed as follows.

### 3.2.1 Surface and bedrock digital elevation model

~~Although the run time of the C-L simulation increases exponentially as the number of grid cells increases, to~~To describe clearly the control process, especially the two dams and levees in the catchment, we unified grid cell scales to 10 m for all ~~needed~~input data of the C-L. The GlobalDEM product with a 10 m × 10 m resolution and 5 m (absolute) vertical accuracy was used ~~as the prepared data~~ to form three types of initial DEMs (UP DEM, PP DEM, and EP DEM). Before rebuilding initial DEMs, we filled the sinks of the original GlobalDEM based on Environmental Systems Research Institute's (ESRI's) ArcMap (ArcGIS, 10.8) to eliminate the 'walls' and the 'depressions' in the cells and avoided the intense erosion or deposition in the early run time. Then the non-sinks DEM was used as the surface DEM in Scenario UP (UP DEM) without any facilities. According to the engineering control project described in Section 3.2.2, ~~Scenario PP's~~ surface DEM of Scenario PP (PP DEM) included the dams by raising the grid cell elevations by 10 m for the dam in upper ~~dam~~stream and 9 m for the dam in the transitional area. Similarly, the surface DEM in Scenario EP (EP DEM) included the dams in PP DEM. In addition, two levees were produced by raising grid cells' elevation by 2 m that were represented at selected locations. ~~Incidentally~~For scenario EP, the placement and setting of vegetation revetments in Scenario EP were introduced in Section 3.2.2.

~~In Section 2.2, the~~The spatial heterogeneity of source ~~materials~~material (Figure 1c) indicates the discrepancy of erodible thickness, which equals the difference between surface DEM (DEM) and bedrock DEM (bedDEM). We divided the study area into five regions according to the erodible thickness ~~into five regions~~ (Fig. S1) by checking out the relative elevation of the foundations of buildings, the exposed bedrock, and the deposited depth of landslides to the ground level. The average thicknesses of upstream low and high-altitude areas were set to 10 m and 3 m, respectively, and the thickness of erodible layer in the downstream area was set to 3 m. For the river channel and outlet, there would be a large amount of deposition, ~~and~~; the thickness of erodible sediment was set to 5 m and 4 m, respectively. ~~The~~As the dams in Scenario PP and the levees in Scenario EP were non-erosive concrete. ~~As such~~, we set the erodible thickness of these features to 0 m. Eventually, DEMs were formatted to ASCII raster as required by C-L. The divided regions varied in erodible thickness, the placement of additional levees and vegetable revetments in Scenario EP, and the generation process of DEMs and bedDEMs were shown in Fig. S1.

### 3.2.2 Vegetation settings

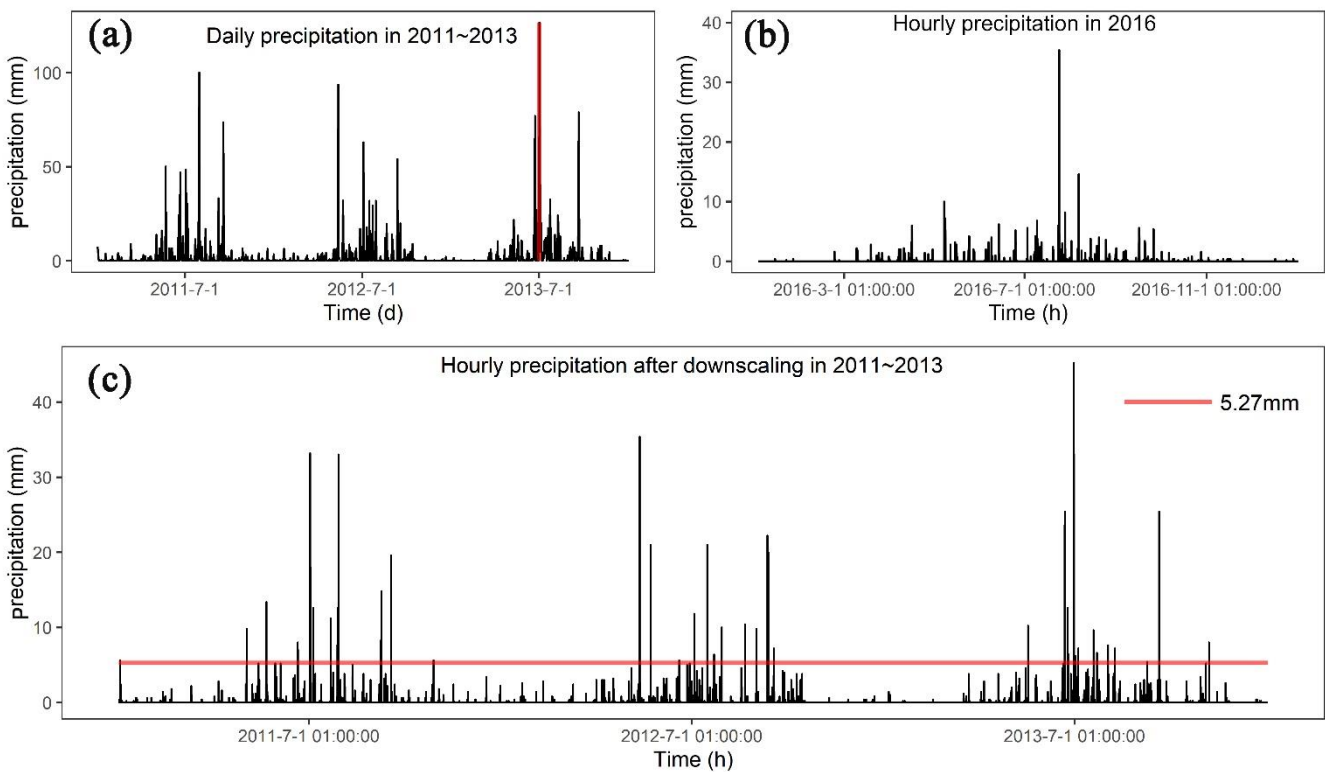
Another parameter required in each scenario simulation was the m value ~~in C-L's~~of hydrological model (TOPMODEL); within C-L, which controls the exponential decline of transmissivity with depth (Beven, 1995, 1997) and influences the peak and duration of the hydrograph in response to rainfall. ~~The lower the m value, the lower the vegetation coverage, and the flashier flood peak and shorter duration are reflected in the flood hydrograph (Coulthard et al., 2002)~~The m value effectively imitates the effect of vegetation on the movement and storage of water within the soil. The lower the m value, the lower the vegetation coverage, and the flashier flood peak and shorter duration are reflected in the flood hydrograph (Coulthard et al., 2002). The m value is usually determined by the landcover (e.g., 0.02 for the forest, 0.005 for the grassland) ~~(Coulthard and Van De Wiel, 2017)~~. ~~In our study, we set the value as 0.008 in our smaller catchment (14 km<sup>2</sup>) in Scenario UP and PP, which resembles the m value of farmland covered with lower vegetation (Coulthard and Wiel, Van De J., 2017).~~ In our study, we set the m value as 0.008 in our smaller catchment (14 km<sup>2</sup>) in Scenario UP and PP, which resembles the m value of farmland covered with lower vegetation coverage in the same catchment studied by Xie et al. (2018) and Li et al. (2018). As mentioned earlier, the upstream-low elevation area covered by the biological measures ~~designed~~ in the EP scenario was assigned a higher m value of 0.02. It has been calibrated in the more extensive catchment containing our study area by replicating the flood event in 2013 (Xie et al., 2018).

199 **3.2.3 Rainfall data**

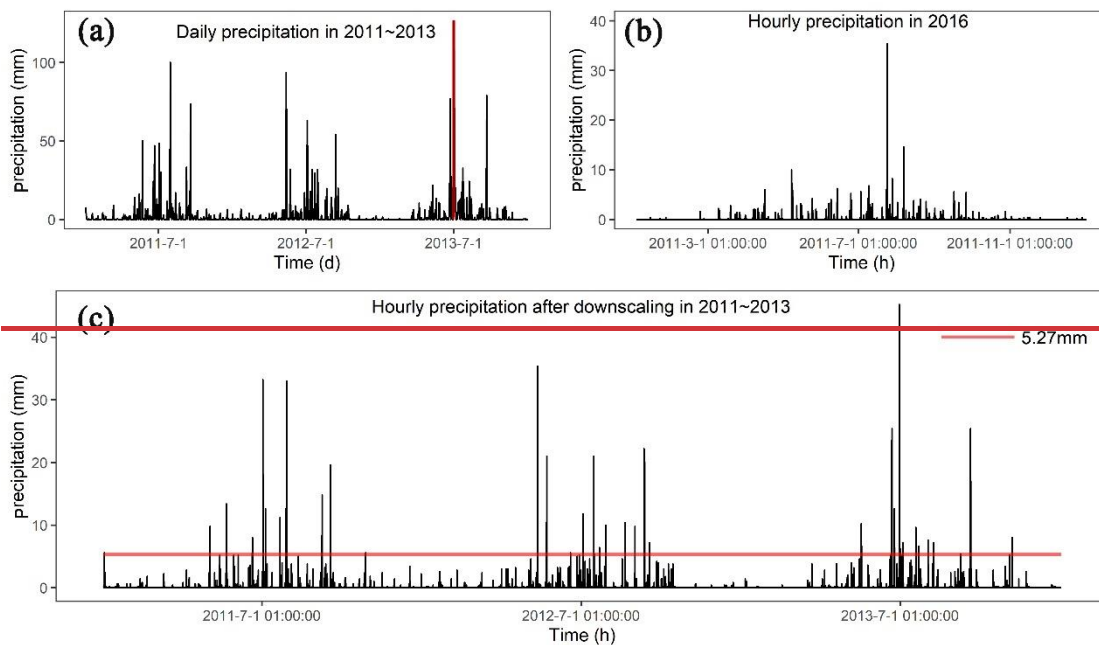
200 In this research, we compared three scenarios with identical precipitation data between 2011 and 2013, as mentioned in section  
 201 3.1. The source data of precipitation in 2011-2013 (Figure 2a) was obtained from the China Meteorological Administration  
 202 (<http://data.cma.cn>) with daily temporal resolution. The rainfall-intensity and ~~the~~ frequency of extreme rainfall events affect  
 203 patterns of erosion and deposition (~~Coulthard et al., 2012b; Coulthard and Skinner, 2016~~)-(Coulthard et al., 2012b; Coulthard  
 204 and Skinner, 2016). Therefore, we used the stochastic downscaling method to generate hourly data to best~~better~~ capture the  
 205 hydrological events ~~in this study, which was~~ introduced by Li et al. (2020) and Lee and Jeong (2014). The referenced hourly  
 206 precipitation was observed from the pluviometer located 20 km from the study area in 2016 (Figure 2b), with an annual total  
 207 precipitation of 684 mm. The observed rainfall in 2016 was characterised by ~~that~~: (1) hourly precipitation was from 1.1 mm to  
 208 35.4 mm, and (2) the maximum and average duration of a rainfall event was 24 h and 2.8 h, respectively. The main processes  
 209 of the downscaling method are:

- 210 ● extracting the hourly rainfall of specific days in 2016 closest to the daily rainfall in 2011-2013 through the threshold  
 211 setting and producing the genetic operators using the extracted hourly rainfall dataset;
- 212 ● mixing on the genetic operators by genetic algorithm (Goldberg, 1989) composed of reproduction, crossover and mutation  
 213 and repeating until the distance between the sum of hourly rainfall and the actual daily rainfall is less than the set threshold;
- 214 ● normalising the hourly precipitation to remain the daily rainfall value unchanged. ~~The input of generated hourly precipi-~~  
 215 ~~tation is catchment lumped in Scenario UP and PP and divided into two separate but identical rainfall in Scenario EP.~~

216 Figure 2c shows the downscaled rainfall series between 2011 and 2013. ~~The downscaled hourly precipitation-rainfall~~ better  
 217 captured the hydrological events ~~on account of at an hourly scale compared to~~ the hourly-mean rain (5.27 mm) ~~in~~on the day  
 218 with extreme rainfall (126.5 mm), which was far from the actual situation. ~~Corresponding to the m value settings, the input of~~  
 219 ~~generated hourly precipitation is catchment lumped in Scenario UP and Scenario PP and divided into two separate but identical~~  
 220 rainfall in Scenario EP.



221



222  
223 **Figure 2: (a) Daily precipitation in 2011-2013 (the red vertical line indicates maximum daily precipitation of 126.5 mm); (b) Hourly**  
224 **precipitation in 2016; (c) Downscaled hourly precipitation in 2011-2013 (the red horizontal line indicates the hourly-mean precipi-**  
225 **tation 5.27 mm ~~in~~ the day with maximum precipitation ~~showed~~ marked in (a)).**

### 226 3.2.4 Other parameters

227 The C-L ~~model~~ is sensitive to a set of input data introduced by [Skinner et al. \(2018\)](#) ~~Skinner et al. (2018)~~ for a catchment with  
228 a grid cell size of 10 m, such as sediment transport formula, slope failure threshold, and grain size set. The grainsize distribu-  
229 tion of sediment is derived from samplings at 14 representative locations in the same study basin by Xie et al. (2018). Given  
230 the grainsize distribution in this study, ~~we selected~~ the Wilcock and Crowe formula was selected as the sediment transport rule,  
231 which was developed from flume experiments using five different sand-gravel mixtures with grain sizes ranging between 0.5  
232 and 64 mm (Wilcock et al., 2003). Considering the steep slope on both sides of deep gullies ~~there distribute, we tended to set,~~  
233 a higher slope failure threshold was determined to replicate the geomorphic changes between 2011 and 2013 ~~realistically~~.  
234 Additionally, we found that the probability of shallow landslides indeed accumulated from 20° to 50° in slope gradient between  
235 2011 and 2013 (Li et al., 2018). The slope angle was derivate from the DEM with a 30 m spatial resolution, which caused a  
236 lower slope angle than that with a 10 m resolution. As such, we set 60°, which is lower than the 65° used in a scenario without  
237 landslides (Xie et al., 2022) and higher than 50°. Some parameters were determined by repeated experiments such as the  
238 minimum Q value, and the other input values were referred to default values recommended by the developers (such as the max  
239 erode limit in the erosion/deposition module and the vegetation critical shear stress) in [https://sourceforge.net/p/caesar-](https://sourceforge.net/p/caesar-lisflood/wiki/Home/)  
240 [lisflood/wiki/Home/](https://sourceforge.net/p/caesar-lisflood/wiki/Home/). Table S2 in the supplemental material presented ~~C-L~~ model parameters of C-L used in ~~the current~~ this  
241 study.

### 242 3.2.5 Model calibration

243 Considering the ungauged basins before 2015, we replicated the flash flood event in July 2018 by using C-L simulations to  
244 calibrate the hydrological components. Based on Scenario PP (with two ~~cheek checking~~ dams), we changed the rainfall series  
245 into input the two-week hourly precipitation in July 2018 (Fig. S2a), which is recorded by the rain gauge located 2.5 km away  
246 from the catchment (Fig. S2b). The simulation results (Fig. S2c and Fig. S2d) ~~represented~~ show the erosion map and maximum  
247 water depth map in Scenario PP on July 15, 2018. As shown in Fig. S2c and Fig. S2d, we selected three locations to compare  
248 the deposition and inundation in simulation results ~~with remotely sensed, satellite~~ images and photos. ~~The comparative results~~  
249 (Fig. S3) ~~revealed the similar ranges of the deposition and inundation between simulation results and remotely sensed images.~~



Additionally, the values of simulated sediment depth/thickness and water depth were close to those measured from images/pictures, which indicated that the flash flood event was well replicated successfully by the C-L using the input data. Table 1 shows three year landscape changes under three different scenarios that were simulated and compared to analyse the intervention effectiveness in 2011-2013.

**Table 1: Scenarios setting**

Scenario	Descriptions	Period	DEM (10m)	Rainfall data
UP	no anthropogenic intervention		UP-DEM UP-bedDEM	downscaled hourly precipitation in the period (lumped)
PP	the present two check dams upstream without dredging work	2011-2013 (3 years)	PP-DEM PP-bedDEM	downscaled hourly precipitation in the period (spilt)
EP	additional vegetation revetments in the source area and levees in the deposit area based on Scenario PP		EP-DEM EP-bedDEM	

### 3.3 Output analysis

The C-L model outputs in each scenario include hourly water and sediment discharge at the basin outlet, the difference between DEMs at a specified time and initial DEMs (EleDiffs), and hourly sediment yield. We validated the model outputs by comparing the hourly discharge and EleDiffs reflecting the depth of sediment deposition or erosion (> 0.1 m: deposition, < -0.1 m: erosion) with field survey materials. The overall temporal and spatial geomorphic changes reflected by EleDiffs under three different scenarios were used to assess the geomorphic response to interventions. To explore the geomorphic response to various control measures, we zoomed in/focused on the key spots placed checking dams, levees, and vegetation revetments and recorded the depth of deposited sediment behind two dams. For To further exploring/explore the spatial heterogeneity, we compared respectively with the volumes of deposition and erosion among three divided regions, including the source area, transitional area, and deposition area.

Based on the visual analysis and quantitative results, we defined two formulae to assess the intervention's effectiveness of intervention. The conservation ability ( $Ca$ , Eq. (3)) was calculated based on variables in the sediment balance system (Figure 3). The sediment volume of deposited sediment ( $D_n$ ) and input sediment from the upper connected region ( $I_n$ ) is equal to that of eroded material ( $E_n$ ) and output sediment to the next part ( $O_n$ ) over the same period (Eq. (1), Eq. (2)) in the system. A higher value of  $Ca$  in a specific region and scenario indicates that a more effective control system is applied.

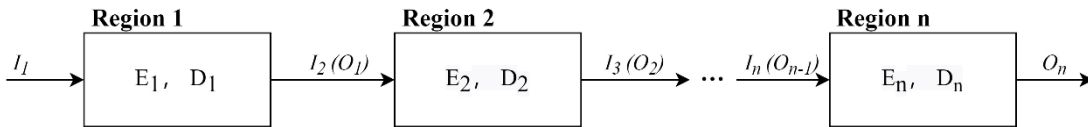


**Figure 3: The sediment balance system in the study area (the Region  $n$  indicated source area, transitional area, and deposit area in this study)**

$$I_n = \sum_2^n E_{n-1} - \sum_2^n D_{n-1}, \quad (1)$$

$$I_n + E_n = O_n + D_n, \quad (2)$$

$$Ca = \frac{D_n}{I_n + E_n} \quad (3)$$

Where,  $n$  is the region number of source area (=1), transitional area (=2), and deposit area (=3).

Additionally, we designed the relative efficiency ( $Re$ , Eq. (4)) to depict how much a set the efficiency of intervention measures in Scenario PP and EP were efficient in sediment loss, with the comparison to Scenario UP.

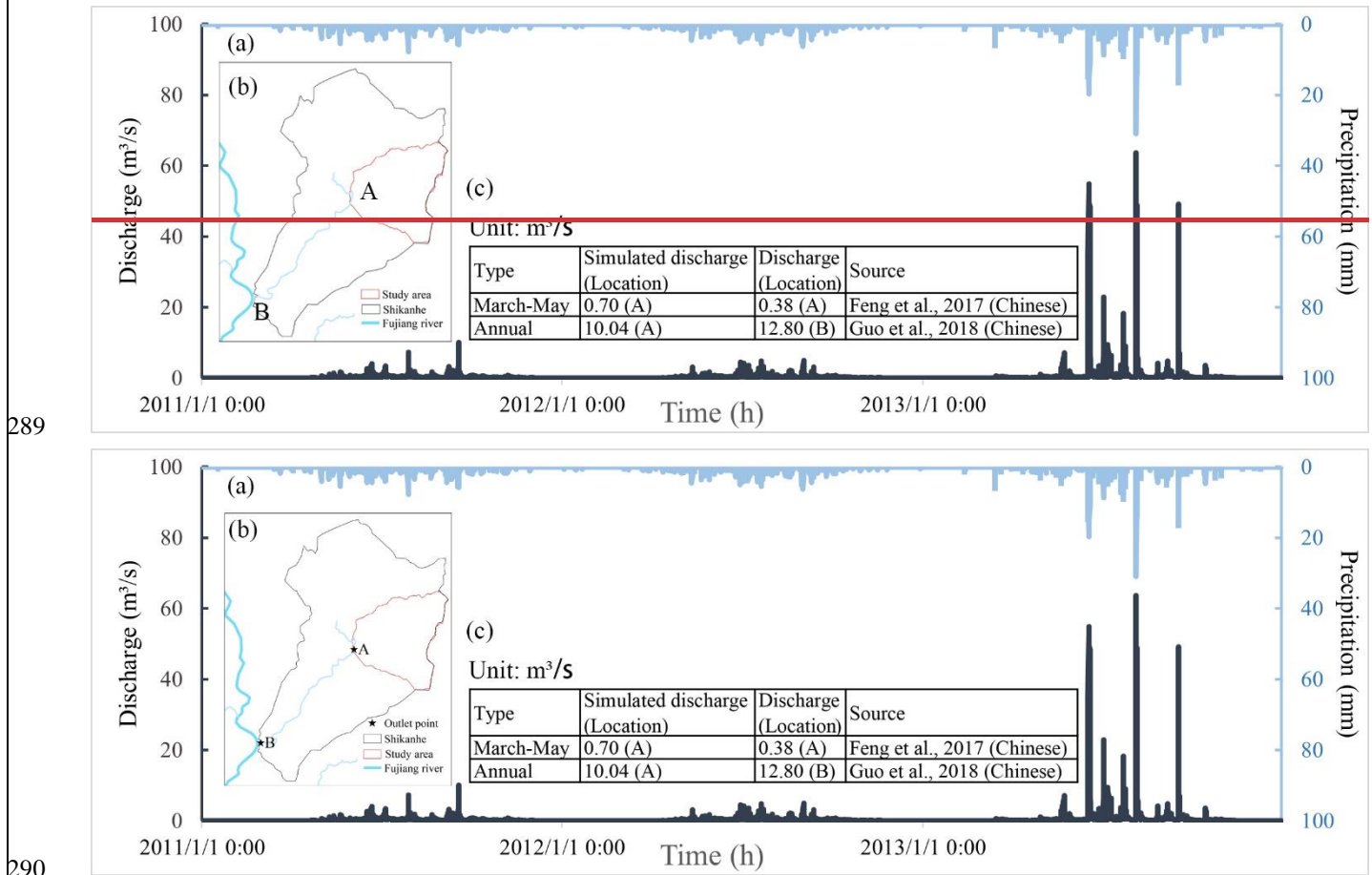
$$Re_{PP/EP,i} = \frac{Q_{UP,i} - Q_{PP/EP,i}}{Q_{UP,i}} \quad (4)$$

277 Where  $i$  is the sequence of the day;  $Q_{UP}$  is the daily sediment yield measured at the catchment outlet in Scenario UP;  $Q_{PP/EP}$  is  
 278 the daily sediment yield measured at the catchment outlet in Scenario PP or Scenario EP of day  $i$ ;  $Re_{PP/EP}$  is the daily relative  
 279 effectiveness of control measures in Scenario PP or Scenario EP.

## 280 4. Results

### 281 4.1 Model verification

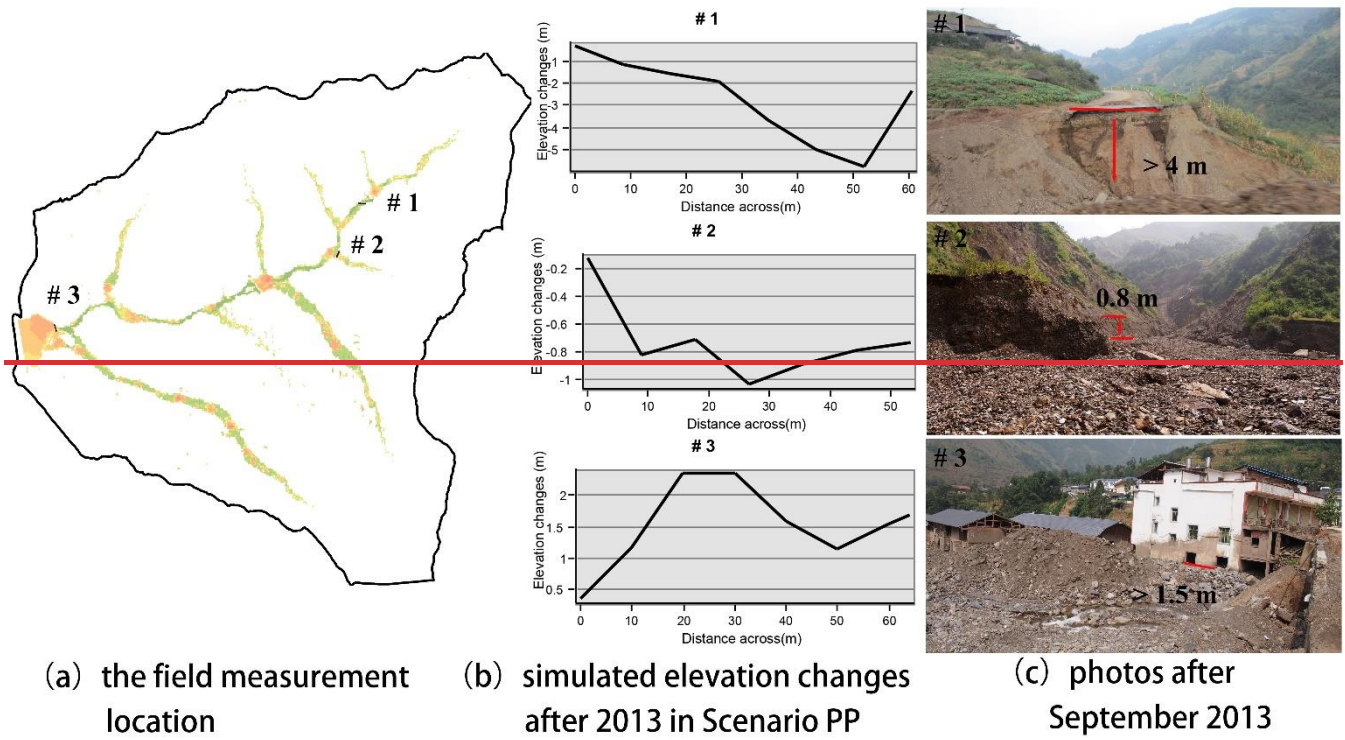
282 Figure 4 shows the input precipitationsrainfall data and modelled discharge hydrograph between 2011 and 2013 (Figure 4a);  
 283 in addition, presents the. The comparison of simulated mean discharge in April through July and the whole year with field  
 284 survey materials in two locations (are also presented (Figure 4-b, c). Concerning the discharge hydrograph, the peak discharges  
 285 ( $63.7$ ,  $54.9$ , and  $50.3 \text{ m}^3/\text{s}$ ) appear identically correspond well with the peak rainfall intensities ( $31$ ,  $19.7$  and  $15 \text{ mm}$ ). The value  
 286 of modelled water discharge from March to May in the catchment outlet (location A) is slightly larger than the measured value  
 287 recordedreported by Feng et al. (2017). Additionally, an average annual discharge of  $10.04 \text{ m}^3/\text{s}$  in location A is less than that  
 288 of  $12.80 \text{ m}^3/\text{s}$  in the catchment outlet (location B), which has an area approximately three times the size of the study area.



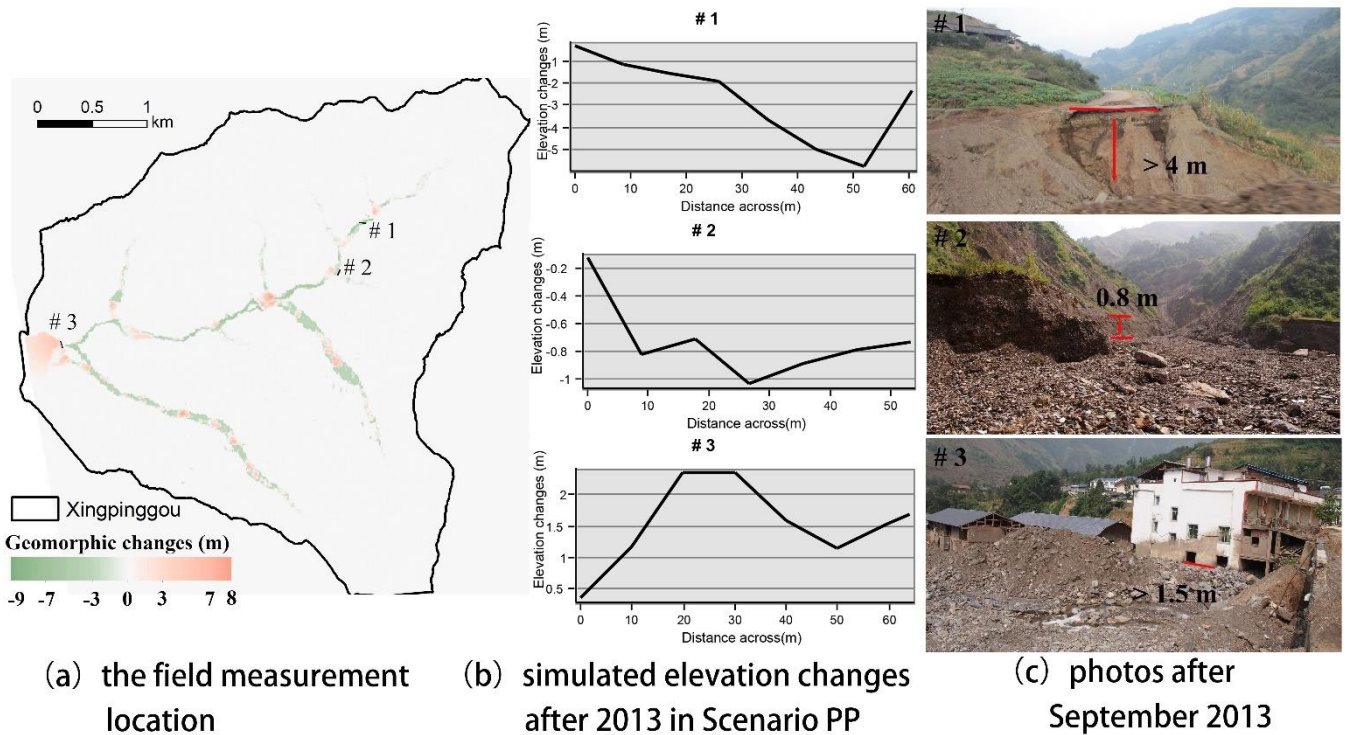
291 **Figure 4: The input and output of the hydrograph.** (a) The input hourly precipitation and simulated discharge in 2011-2013 in  
 292 Scenario PP; (b) Location of the specified locations to verify outlet point; (c) the comparison of the simulated average discharge to  
 293 the recorded discharge.

294 Figure 5 compares typical Typical cross-sections to the site photos are generated (Figure 5) based on the replicated landscape  
 295 changes in Scenario PP. The first site is located on the upriver road, which was eroded to at a depth of  $5.7 \text{ m}$  according to the  
 296 simulation results, while the photo shows a depth of no less than  $4.0 \text{ m}$  without an apparent eroded base. The cross-section #2

297 and site photo of the gully ~~labelled 2~~ depict that the eroded depth is approximately 1.0 m. Meanwhile, a clear sediment bound-  
 298 ary is found in the building located at the deposited area, ~~(# 3)~~, indicating a slightly lower deposition depth than the modelled  
 299 one.



300



301

302 **Figure 5: The comparison of cross-sections from the simulation results to the ~~photos in the field measurement locations~~ measure-**  
 303 **ments after 2013 in Scenario PP.**

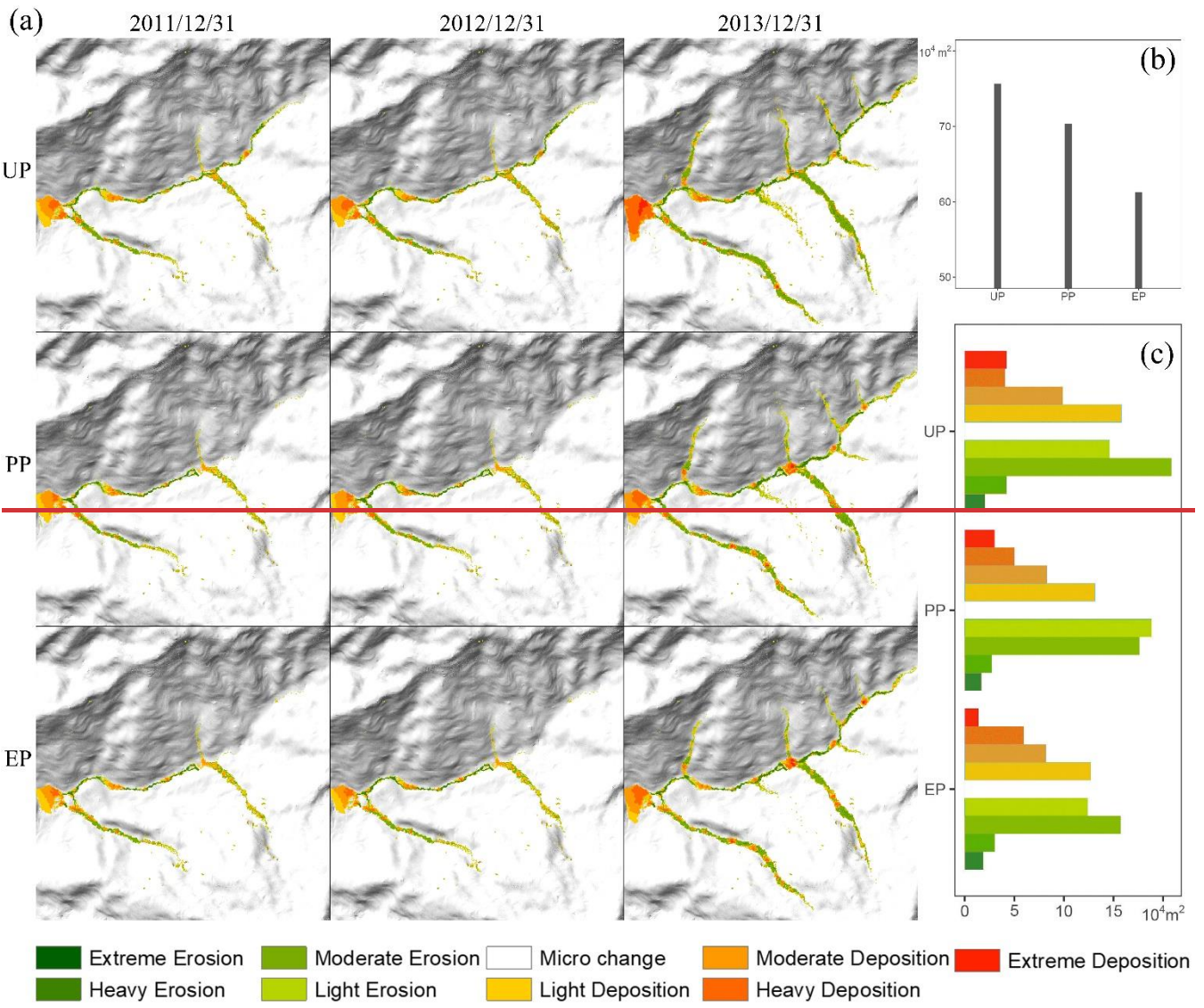
304 **4.2 Overall geomorphic changes**

305 Figure 6a ~~shows compares~~ the three annual landscapes changes in each scenario, which were classified into ~~seven ranks~~ nine  
 306 categories by natural breaks for EleDiffs: extreme erosion (<-7 m), heavy erosion (-7--3 m), moderate erosion (-3--1 m), light

307 erosion (1-0.1 m), micro change (-0.1-0.1 m), light deposition (0.1-1 m), moderate deposition (1-3 m), heavy deposition (3-7  
308 m), and extreme deposition (>7 m). A similar spatial pattern of erosion is observed in all three scenarios. ~~In detail~~ More specif-  
309 ically, erosion mainly occurred ~~mainly~~ in the main channel and the ~~branches on both sides~~ branch valleys, among which the  
310 left branches were more severe. In contrast, the deposition distribution appeared to be varied in three scenarios, especially the  
311 area behind the two dams ~~showed~~ shown in Scenario PP and EP.

312 The total area of affected grid cells representing erosion and deposition in each scenario was calculated to reveal the difference  
313 (Figure 6b). ~~As shown in Figure 6b, the~~ The affected area in Scenario UP was the largest at about 0.76 km<sup>2</sup> (5.4% of the  
314 total catchment), which was larger than that in Scenario PP (0.70 km<sup>2</sup>, 5.0% of the whole catchment), and the affected area  
315 decreased to 0.61 km<sup>2</sup> (4.4% of the total catchment) in Scenario EP. The total area of erosion and deposition reduced gradually  
316 as with more controlling measures ~~were~~ established in this study.

317 Figure 6c compares the extent of geomorphic changes in three situations using the areas varied in depth. ~~Erosion in the three~~  
318 ~~scenarios was similar in that the~~ The light and moderate erosion areas were more than the extreme and heavy ~~erosion areas. ones~~  
319 for all three scenarios. The area size of each erosion degree in UP was more extensive than in PP and ~~larger than in~~ followed by  
320 EP. In addition, the greater the deposition depth, the less deposition coverage. Especially the extreme deposition area was  
321 somewhat more than the area of the heavy deposition in UP. Further analysis shows that extreme, moderate, and light deposition  
322 areas decreased in the order of UP, PP, and EP. The heavy deposition areas show the opposite trend, mainly ~~contrib-~~  
323 uting attributed to the checking dams and vegetation revetments.



324

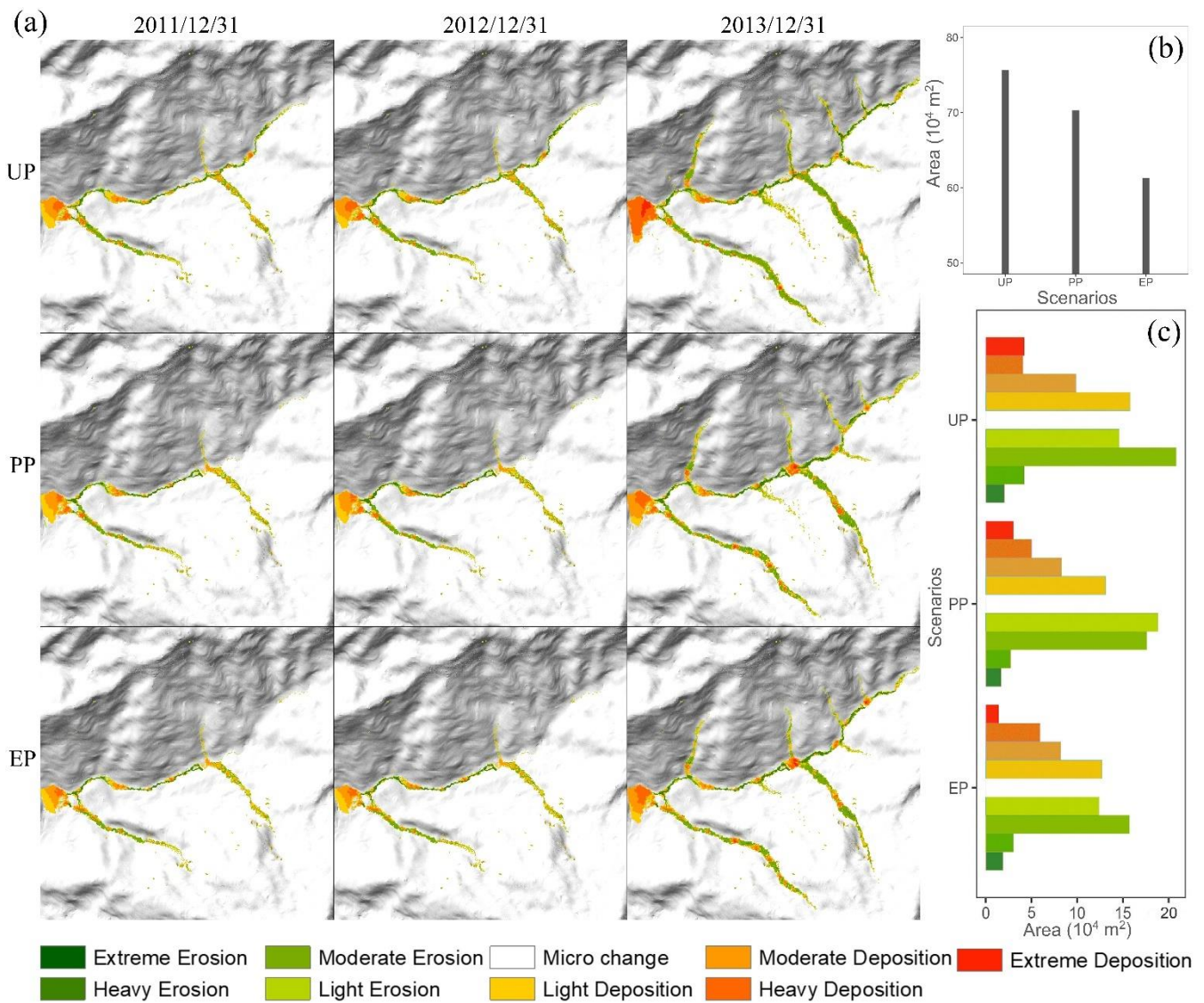


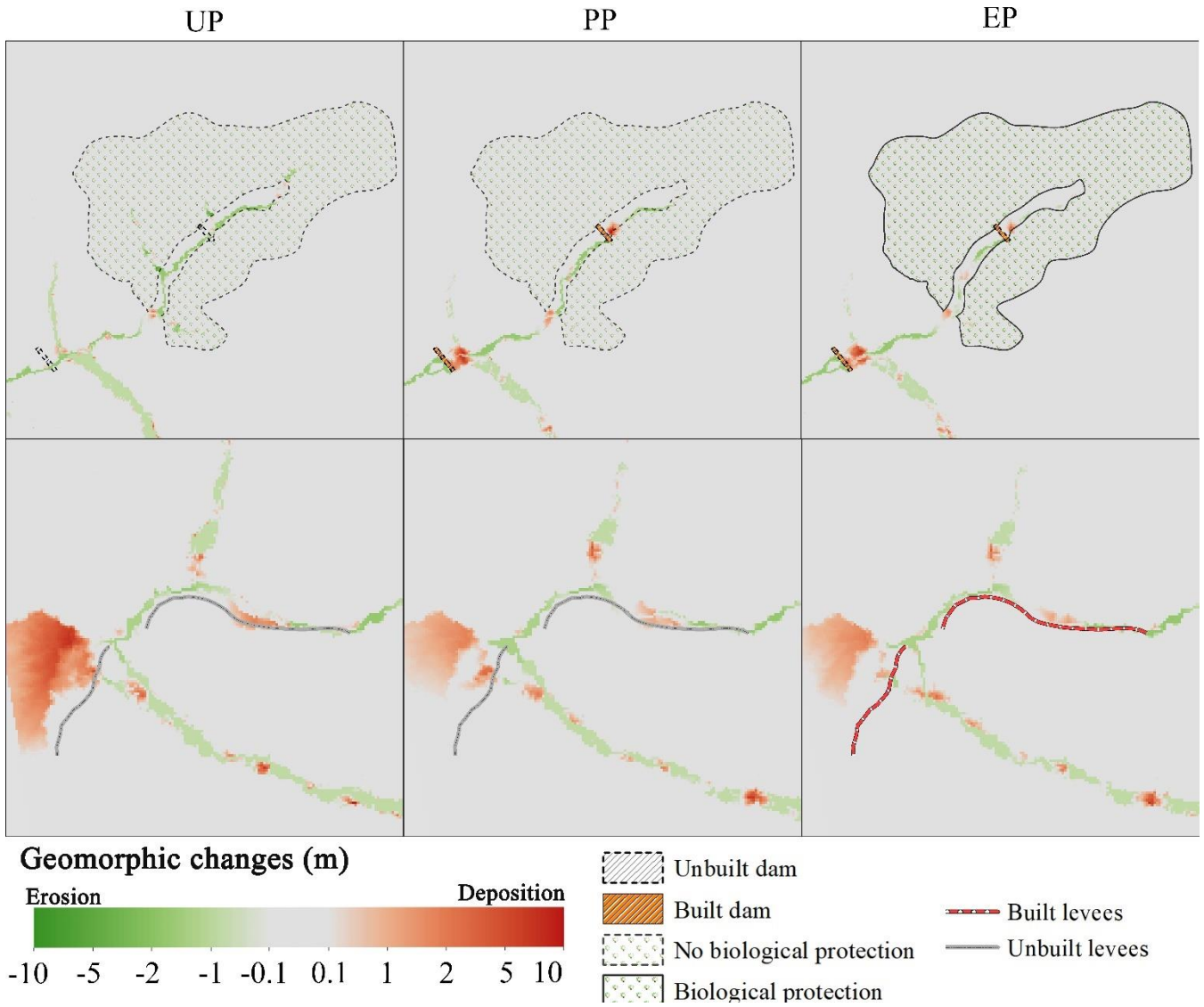
Figure 6: (a) Simulated ~~internal~~ geomorphic changes over time for three scenarios; (b) the affected area ~~included deposition and erosion for three scenarios~~; (c) ~~the ranks of deposition and erosion for three scenarios~~; (c) columnar distribution of different erosion and deposition levels.

### 4.3 Details of key spots

As shown in Figure 7, ~~we provide a detailed investigation of~~, the controlling measures and surroundings for the three scenarios. ~~were further investigated.~~ Behind the two dams upriver, the evident orange clusters indicate that the deposition ~~appeared~~occurred in Scenario PP and EP. In contrast, these locations were dominated by erosion, shown in green in scenario UP. Further analysis of the sediment depth shown in Figure 8 showed that the ~~values of~~ deposited depth behind the dams in Scenario EP ~~were~~was lower than those in Scenario PP. Additionally, in Scenario PP, sediment trapped by dam 1 was ~~lower~~less than that by dam 2, but both ~~with have deposit thicknesses of~~ more than 10 m ~~deposition, which~~ exceeded the dams' heights (~~the dam 1's height is 10 m, the dam 2's height is 9 m~~ finally. At the conclusion of). As for the simulation results in Scenario EP, the values of deposition depth behind the two dams were nearly 8 m, which were lower than the dams' heights.

The ~~materials~~material produced from upriver tributary gullies varied ~~by due to~~ the additional biological protection measures in three scenarios. A volume of  $14.4 \times 10^4 \text{ m}^3$  sediments was transported from EP's biological protection area (solid lines in Figure 7). ~~The loose materials were~~  $27.1 \times 10^4 \text{ m}^3$  and  $16.9 \times 10^4 \text{ m}^3$ , ~~respectively, loose material~~ were produced in the same region without biological protection in Scenario UP and PP, respectively. The vegetation revetment enhanced the sediment conservation based on the role of dam 1. Compared with the deposition in UP and PP without levees in the downriver area (shown in

343 the bottom row of Figure 7; the levees in EP blocked debris in the bend of the channel and played an essential role in  
 344 protecting the residents and cultivated land behind the levees.



345  
 346 **Figure 7: Geomorphic changes at the conclusion key spots of the simulation at key spots results for the UP, PP, and EP scenarios. The**  
 347 **top row is the upriver section extent containing dam 1, dam 2 and the vegetation revetment. The bottom row is the downriver section**  
 348 **extent containing levees.**

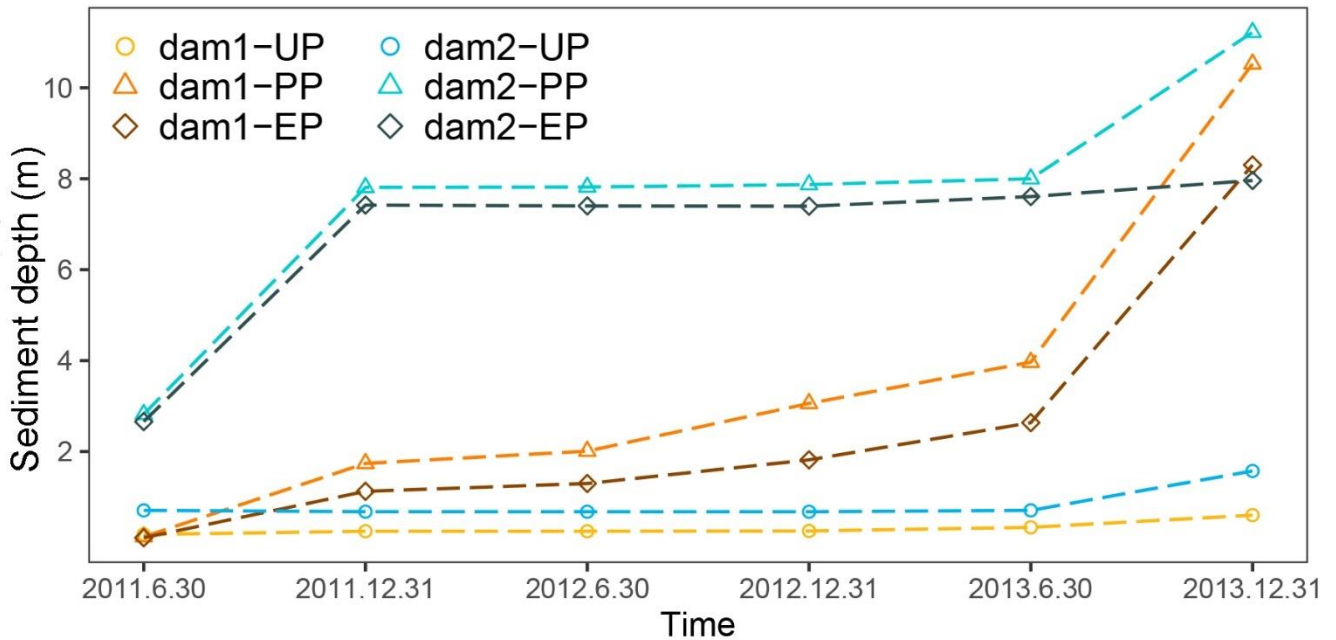
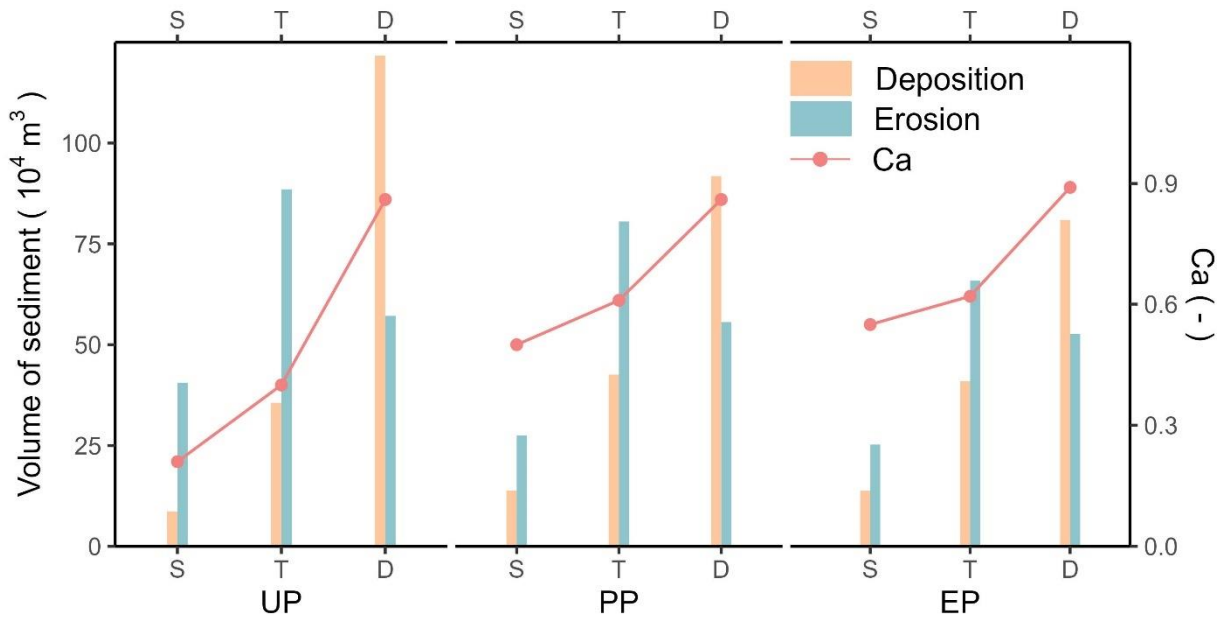


Figure 8: The depth of deposited sediment in the dams' placements.

#### 4.4 Effectiveness assessment of intervention measures

Figure 9 shows the erosion and deposition volumes in the source, transitional, and deposit areas and compares conservation ability ( $Ca$ ) in each scenario. ~~The data showed similar phenomena in~~ For all three scenarios. For example, the deposition volume in the source area was less than that in the transitional area, and the largest amount of sediment was deposited in the deposit area. Regarding the eroded sediment, the largest volume was in the transitional area, followed by the transitional area, and the ~~least was in the~~ source area. presented the least volume. Moreover, sediment transport ~~could be~~ was best controlled ~~the best~~ in the deposit area and ~~the worst~~ contained in the source area ~~in~~ under any intervention conditions. ~~By comparing~~ Compared with the  $Ca$  of the source area in Scenario UP, the value was increased by 138.1% in Scenario PP, which was ~~responsible for~~ attributed to the dam1. ~~And then~~ Likewise, dam 2 in the transitional area reduced sediment loss effectively, which was reflected by ~~the~~ 52.5% increase in  $Ca$ . Furthermore, the mitigation measures in Scenario PP with vegetation revetment and levees in Scenario EP worked better. The conservation ability in the source area increased by 161.9%, due to the dam retainment and vegetation revetment, and the levees helped increase by 3.49% in the deposit area. ~~Therefore, the dams are most effective in blocking sediment. The vegetation revetments strengthen the conservation ability, while the levees are helpful but with a discernable impact on sediment conservation.~~





365

366

367

**Figure 9: The volumes of sediment and the conservation ability ( $Ca$ ) in three areas ~~in~~for each scenario (S: source area; T: transitional area; D: deposit area).**

368

369

370

371

372

373

~~Figure 10 presents the~~The cumulative sediment yield time series for each scenario and the relative efficiency of scenario UP and EP. ~~are present in~~ Figure 10b and Figure 10a, respectively. The steep curve of output cumulative sediment means a significant increase ~~of in the~~ deposition, ~~and three~~. ~~Three~~ increasing stages ~~have high consistency~~are consistent with the rainfall intensity in three monsoons (May-September). The total sediment output in UP was the largest, ~~about of~~  $\sim 30.4 \times 10^4 \text{ m}^3$ , ~~and the total production followed by sediment yield in PP ( $26.3 \times 10^4 \text{ m}^3$ ) was larger than that in~~, and EP presented the least figure ( $19.3 \times 10^4 \text{ m}^3$ ).

374

375

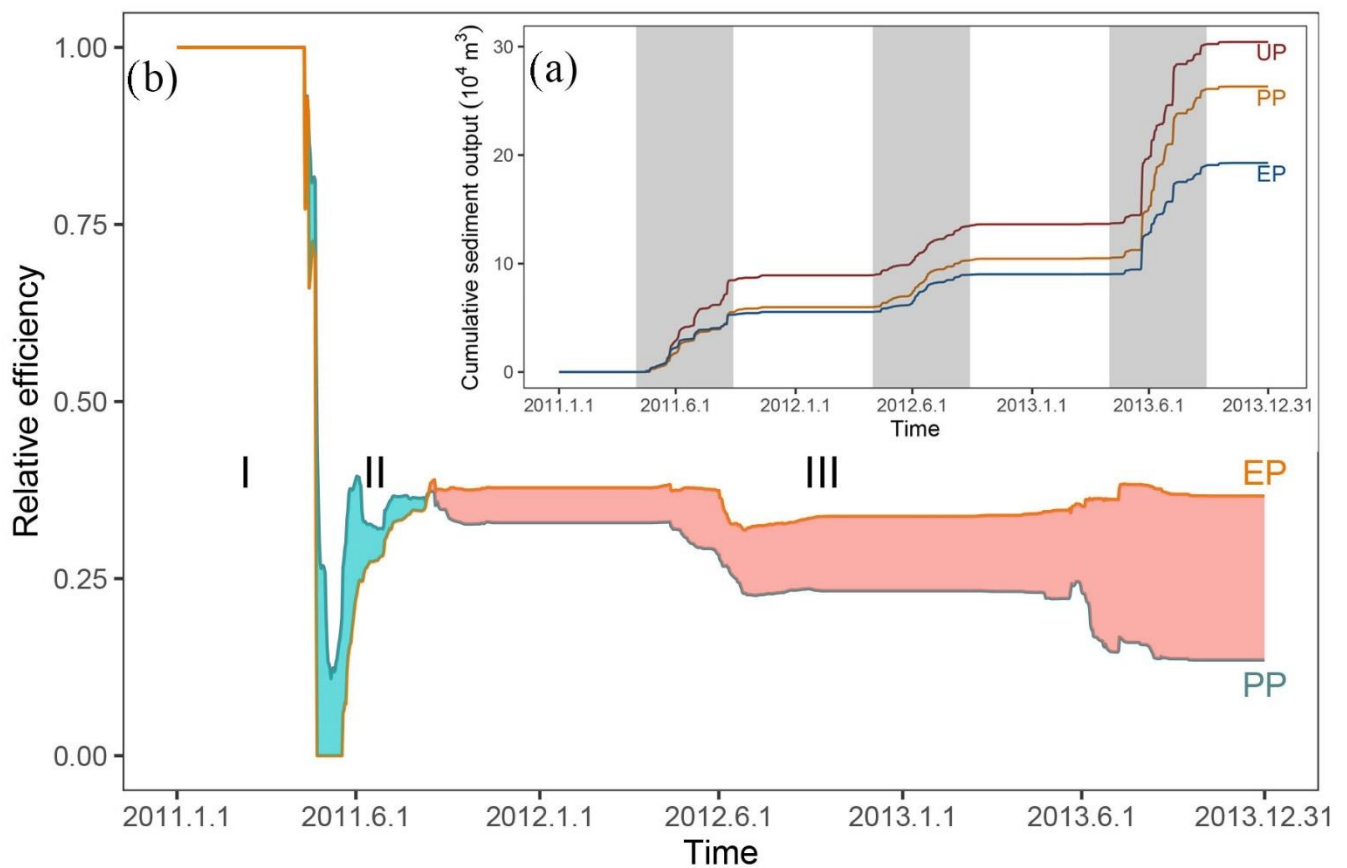
376

377

378

379

The relative efficiency over the period of controlling measures by human intervention in PP and EP (Figure 10b) indicates three distinct stages. Stage I shows that the intervention measures in both scenarios prevented the sediment transport completely. Later stage II is a peculiar period when the effect of enhanced protective measures in EP was not as good as that in PP through repeated experiments, ~~which the increasing complexity of the model would cause. In~~. For stage III, the relative efficiency of the intervention measures in EP was greater than that in UP ~~for a more prolonged stage III~~, which could achieve ~~the~~ long-term effect and stable conservation of solid ~~materials~~material.



380

381 Figure 10: (a) showing the cumulative output sediment over time (grey region highlighting three monsoons), (b) showing the  
 382 relative efficiency of scenario UP and EP compared with the UP (cyan shading represents when PP is more effective than EP and red  
 383 shading represents the opposite)

## 384 5. Discussion

### 385 5.1 Model calibration and uncertainty and application

386 The calibration and uncertainty are essential issues in the CAESAR-Lisflood (C-L) simulation of the geomorphic response to  
 387 intervention measures (Yeh and Li, 2006). A preliminary calibration was carried out by replicating the geomorphic changes  
 388 and water depth driven by an extreme rainfall event that occurred in 2018. The results (Fig. S3) demonstrated that the C-L  
 389 successfully replicated the flash flood event using the initial conditions and model parameters. Actually, the calibration of the  
 390 replicating ability of the geomorphic response to intervention measures was derived from a direct comparison between model  
 391 results and direct measurements (Figure 4 and Figure 5). As a result, the simulated water discharge was more than the measured  
 392 one but with the same order of magnitude. Moreover, the errors of erosion and deposition depth between simulation in Scenario  
 393 PP and photographic evidence in three locations were at most 20%. The results suggest the robustness of the model settings  
 394 and parameterisation.

395 The source of uncertainty is mainly from the model parameters and driving factors. Skinner et al. (2018b) provided a detailed  
 396 sensitivity analysis of C-L, indicating that the sediment transport formula significantly influences a smaller catchment mod-  
 397 elled by 10 m-grid cells. The sediment transport law, Wilcock and Crowe equations (Wilcock et al., 2003) have been proven  
 398 suitable in the Xingping valley (Xie et al., 2018, 2022a, b; Li et al., 2020). Nevertheless, the empirical models of sediment  
 399 transport would overpredict bedload transport rates in steep streams (gradients greater than 3%) (D'Agostino and Lenzi, 1999;  
 400 Yager et al., 2012). Additionally, the driving factor, the input hourly rainfall data downscaled from the daily sequence is an  
 401 unrealistic situation. Various sediment transport equations and downscaled hourly rainfall data need to be tested in C-L to  
 402 determine the uncertainty further.

## 403 5.2 Intervention effects

404 The more facilities equivalent to more comprehensive intervention systems in this study aim to control sediment delivery. The  
405 C-L simulation of the geomorphic response to intervention measures suggests considerable influence on spatial modification  
406 and sediment yield. The relative systematic measures lead to fewer total affected areas (7.9%-19.7%) and sediment yield  
407 (16.7%~36.7%), which are suggested in overall evidence (see Figure 6 and Figure 10). Such catchment-scale performance  
408 disturbed by the extreme event is in line with the viewpoints of other authors (Chen et al., 2023; Lan et al., 2020; Chen et al.,  
409 2015).

410 The mitigation measures considerably changed the soil conservation ability in three sub-regions, especially in the source area.  
411 Herein, two main reasons why the erosion material is less in the source area than in another two sub-regions are inferred from  
412 the interactions of loose material and topographic constraints. First, the abundant loose solid material formed by the strong  
413 earthquake have stabilised overall since 2008's debris flow (details in Table S1). Second, the long and deep gullies are mainly  
414 located in the transitional area (Yaogouli, Shicouzi, Yangjiashan) and deposit area (Qinggangping), which provide more sedi-  
415 ment supply than the source area. As shown in Fig. S4, the movement of the material occurred mainly in the branch valleys in  
416 the transitional and deposit area.

417 Moreover, comparing details and conservation ability with three scenarios stressed the unique role played by different inter-  
418 vention measures. For example, the check dams are most effective in blocking sediment, and the vegetation revetments  
419 strengthen the conservation ability. The synergy effect of soil conservation ability of checks dams and vegetable coverage is  
420 created with an increase of more than two times. The levees are barriers with a discernable impact on sediment conservation  
421 but with a special specific object-oriented protection.

422 The effectiveness of mitigation measures detected will decrease over time with a smaller downward trend. We supplement a  
423 ten-year experiment to reveal the decreasing trend over a more extended period. We randomly selected one of the 50 repeated  
424 rainfall datasets (year 2016-year 2025) downscaled by Li et al., 2020, which were generated from NEX-GDDP product (spatial  
425 resolution: 0.25°×0.25°, temporal resolution: daily) under RCP 4.5 emission scenario. The extracted rainfall sequence was then  
426 input to C-L to simulate the effectiveness of three intervention scenarios. The result (Figure 11) illustrates that stage III (the  
427 stable stage that started on the 161st day, in which Scenario EP's intervention measures were more effective) lasted longer than  
428 stages I and II, which were only at the start. The relative effectiveness in both PP and EP scenarios decreased gradually, while  
429 the curve fell faster in PP than in EP.

430 The storage capacity of checking dams fades as the accumulation of sediment deposits, which necessarily lead to the gradual  
431 decrease of intervention effectiveness. Additionally, the vegetation revetments remain operationally effective in reducing sed-  
432 iment transport by stabilising topsoil over the period when the role of dam reservoirs gradually fails due to the lack of dredging  
433 work. Therefore, the vegetation protection strategy is vital for “green development” to reduce sediment loss but requires further  
434 efforts.

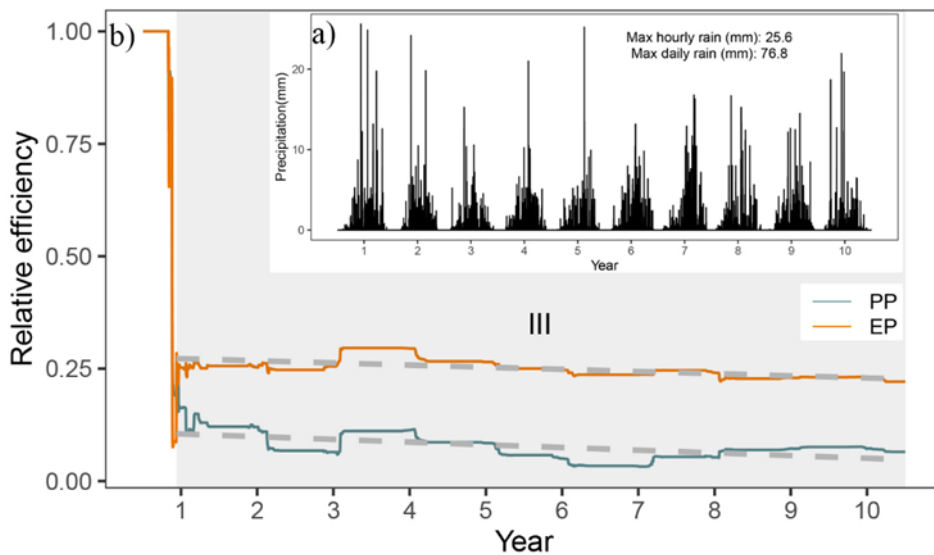


**Figure 11: Future rainfall input and relative efficiency of sediment intervention measures. (a) rainfall downscaled from stochastic future rain; (b) the relative efficiency changes over ten years (grey region highlighting stage III, and the grey dashed lines indicating the linear fitting curve).**

## 5.2 Limitations and applications

We built the dams and levees in our simulations by increasing the elevation in the expected location and assuming that it could not be eroded (see <https://sourceforge.net/projects/caesar-lisflood/>). This method proved experimentally feasible (Poepl et al., 2019; Gioia and Schiattarella, 2020). The rigid dam and levee body embedded in the model would not be broken or weakened over time so the simulation result could underestimate the geo-hazard risk. Considering the complexity of the geo-hazard mechanism, the abovementioned tools could not simulate the occurring process of geo-hazard chain links. They would ignore the fierce attack on the environment and facilities downstream. Some typical geo-hazard chains were focused on the specified event in a short time and recreated the hazard lifecycle using physical and mechanical models. Uncertainty deserves a discussion for understanding and implementing the simulation results in most geographical analyses and modelling processes (Yeh and Li, 2006). Comparative simulation tests using the C-L tool suggested a complex spatial and temporal evolution of sediment transport. They demonstrated that the efficiency varied in scenarios, which differed in control measures conducted on the mountainous areas susceptible to secondary geo hazards. In this study, we cited local research and comprehensive parameter sensitivity papers for the parameters involving geological conditions. We downscaled the daily rainfall sequence into hourly data collected in 2016 for every year because the total rainfall and intensity were identified as a 'normal year' in 2016 (Xie et al., 2018). Although the intensity and event time would not be the same as the actual value for the generated input data, the realisation of total rainfall in three different years suggested reasonable differences.

(Fan et al., 2020).

The methods applied in the study further demonstrate the role of that C-L as an effective tool to understand for understanding the short-medium term or long-term geomorphology changes (Ramirez et al., 2022; Li et al., 2020; Coulthard et al., 2012a) (Ramirez et al., 2022; Li et al., 2020; Coulthard et al., 2012a) and observe observing the effectiveness of natural hazard interventions measures provided under different rainfall patterns. For example, Our simulations indicate that the mitigation facilities in this study were effective, especially engineering efforts cooperating with vegetation revetments in the upstream area, which would help decision-makers to optimise the management strategies to control mountain disasters. Geotechnical engineering has disadvantages, even though it is a mature technology that identifies and fixes problems quickly (Cui and Lin, 2013), such as the greater work and expense and the difficulty of maintenance. While the 'green development' "green development", the vegetation cover was effective in preventing erosion by strengthening topsoil and absorbing excess rainwater with its roots

465 (Reichenbach et al., 2014; Stokes et al., 2014; Forbes and Broadhead, 2013; Mickovski et al., 2007). Alternatively, the methods  
466 could be used to study the tree planting patterns on different slopes.

### 467 **5.2 Short-medium term problem**

468 ~~We used an ingenious and simple method to build the dams and levees in the simulation by increasing the elevation in the~~  
469 ~~expected location and assuming that it could not be eroded (see <https://sourceforge.net/projects/caesar-lisflood/>). This method~~  
470 ~~proved to be experimentally feasible (Gioia and Schiattarella, 2020; Poeppel et al., 2019). The rigid dam and levee body~~  
471 ~~embedded in the model would not be broken, and the effect would not weaken, so the result of the geo-hazard risk assessment~~  
472 ~~would be reduced to some extent. Although the short and large number of moving debris triggered a tremendous impact in the~~  
473 ~~simulation, the tools could not simulate the geo-hazard chain links. They would ignore the fierce attack on the environment~~  
474 ~~and facilities downstream. Some typical geo-hazard chains were focused on the specified event in a short time and recreated~~  
475 ~~the hazard lifecycle using physical and mechanical models (Fan et al., 2020). We concentrated on the effectiveness of mitiga-~~  
476 ~~tion measures in the short-medium term, which is different from those in space-time scales and purposes. Therefore, the three-~~  
477 ~~year simulation time made it underestimated risk assessment and success to simulate the effect of mitigation measures com-~~  
478 ~~pared with the actual result in this study.~~

### 479 **5.3 Sediment transport patterns**

480 ~~Unlike the typical debris flow research, where three divided areas get their names for the materials process, the simulation~~  
481 ~~result demonstrated that the loose solid materials from the source area sliding to the resting area were the least among the three~~  
482 ~~regions, even for the scenario UP (unprotected landscapes). The sediment transport patterns change considerably. First, the~~  
483 ~~abundant loose solid materials formed by the strong earthquake have stabilised generally since 2008's debris flow (details in~~  
484 ~~Table S1). Second, the long and deep gullies are mainly located in the transitional area (Yaogouli, Shicouzi, Yangjiashan) and~~  
485 ~~deposit area (Qinggongping), which provide more sediment supply than the source area. As shown in Fig. S4, the movement~~  
486 ~~of the materials occurred mainly in the branches in the transitional and deposit area. Moreover, the mitigation measures inter-~~  
487 ~~vened in surface process, which lead to the changes in erosion and deposition in three areas. For example, an increase of~~  
488 ~~deposition and a reducing of erosion appeared to be in source and transitional area, while the sediment deposition reduced~~  
489 ~~significantly in deposit zone.~~

### 490 **5.4 Long-term effectiveness**

491 ~~In the warmer world, with more water vapour in the atmosphere, precipitation extremes will intensify, increasing the likelihood~~  
492 ~~of extreme and intense rainfall (East and Sankey, 2020). Then sequential increased fluvial transport capacity and erosion would~~  
493 ~~accelerate geomorphic changes. With increased uncertainty of precipitation and temperature, future work on the landscape~~  
494 ~~evolution of three scenarios will help to understand the long-timescale effectiveness of intervention measures. We randomly~~  
495 ~~selected one of the 50 repeat datasets downscaled by Li et al. (2020), which were generated in 2013–2025 and RCP4.5 emission~~  
496 ~~scenario from NEX-GDDP (spatial resolution:  $0.25^\circ \times 0.25^\circ$ , temporal resolution: daily) to simulate the effectiveness in three~~  
497 ~~scenarios. The result (Figure 11) illustrated that stage III (the stable stage that started on the 161st day, in which Scenario EP's~~  
498 ~~intervention measures were more effective) was more than stages I and II, which were only in the beginning. The relative~~  
499 ~~effectiveness in both scenarios decreased gradually, and the curve went down faster in PP than in EP.~~

500 ~~We further explain the change in intervention effectiveness over time. The effectiveness of controlling sediment transport is~~  
501 ~~primarily for two reasons. The first one concerns the sediment trapping capability of checking dams and the increase of soil's~~  
502 ~~infiltration capacity with vegetation roots. Another is because of the positive feedback about the geomorphic changes, espe-~~  
503 ~~cially the deposition behind the dams. Because the gradient of the upriver channel is slowed down by checking dams, and the~~  
504 ~~sediment carry capacity from the flow is reduced (Luan et al., 2022; Hassanli and Beecham, 2013). The storage capacity of~~

checking dams fades as the accumulation of sediment deposits, which necessarily lead to the gradual decrease of intervention effectiveness. Additionally, the vegetation revetments still reduce sediment transport by stabilising topsoil over the period when the reservoirs are filling with sediment without dredging work. Therefore, the effectiveness of compound measures in Scenario EP goes down with a gentler downward trend.

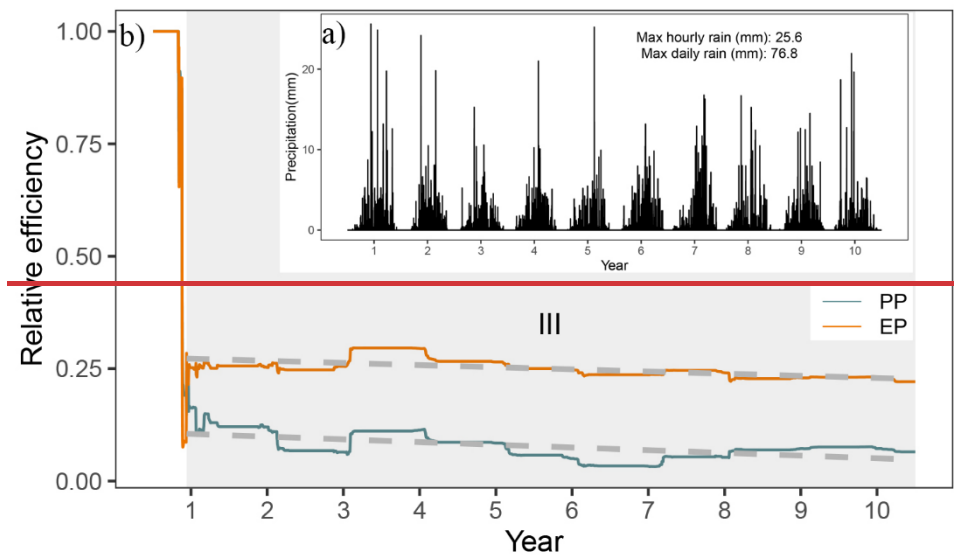


Figure 11: (a) rainfall downscaled from stochastic future rainfall; (b) the relative efficiency changes over ten years (grey region highlighting stage III, and the grey dashed lines indicated the linear fitting curve)

## 6. Conclusions

In this study, we compared the scenarios intervened by check dams, biological measures and artificial barriers are simulated using the C-L model to outline the affected erosion and deposition area, measure the impacts of blocking sediment, and examine how the vegetable revetments helped to stabilise the slope. We have four key findings: are concluded. First, the engineering works measures in controlling sediment transport are efficient, and it would be better at the performance in protecting the fragile environment effectively would be improved combined with other intervention measures like vegetation revetment and artificial barriers. Second, the effectiveness of conservation and mitigation measures would decrease over time. Third, the characteristics of sediment transport patterns changed considerably by caused of the intervention measures. The stabilising sediment ability in the source area increased by 161.9% with the additional help effect of vegetation revetments. At last, the present intervention measures are inadequate to reduce erosion and should be combined with dredging work.

## Declaration of interest statement

The authors declare that they have no known competing financial interests or personal relationships that could have appeared to influence the work reported in this paper.

## Author contribution

Di Wang: Conceptualisation, Methodology, Software, Writing-original draft preparation. Ming Wang and Kai Liu and Jun Xie: Supervision, Methodology, Writing- Reviewing and Editing, Validation.

528 **Acknowledgments**

529 **Acknowledgements**

530 This research was supported by the National Key Research and Development Plan (2017YFC1502902). The financial support  
531 is highly appreciated. The authors would also like to thank Professor Tom Coulthard and his team for their excellent work on  
532 the freely available C-L model (<https://sourceforge.net/projects/caesar-lisflood>).

533

- 535 Bates, P. D., Horritt, M. S., and Fewtrell, T. J.: A simple inertial formulation of the shallow water equations for efficient  
536 two-dimensional flood inundation modelling, *J. Hydrol.*, 387, 33–45, <https://doi.org/10.1016/j.jhydrol.2010.03.027>, 2010.
- 537 Batty, M. and Xie, Y.: Possible urban automata, *Environ. Plan. B Plan. Des.*, 24, 175–192, <https://doi.org/10.1068/b240175>,  
538 1997.
- 539 Beven, K.: Linking parameters across scales: subgrid parameterizations and scale dependent hydrological models, *Hydrol.*  
540 *Process.*, 9, 507–525, <https://doi.org/https://doi.org/10.1002/hyp.3360090504>, 1995.
- 541 Beven, K.: TOPMODEL: A critical, *Hydrol. Process.*, 11, 1069–1085, [https://doi.org/https://doi.org/10.1002/\(SICI\)1099-](https://doi.org/https://doi.org/10.1002/(SICI)1099-)  
542 [1085\(199707\)11:9<1069::AID-HYP545>3.0.CO;2-O](https://doi.org/https://doi.org/10.1002/(SICI)1099-1085(199707)11:9<1069::AID-HYP545>3.0.CO;2-O), 1997.
- 543 Beven, K. J. and Kirkby, M. J.: A physically based, variable contributing area model of basin hydrology, *Hydrol. Sci. Bull.*,  
544 24, 43–69, <https://doi.org/10.1080/02626667909491834>, 1979.
- 545 Chen, N., Zhou, H., Yang, L., Yang, L., and Lv, L.: Analysis of benefits of debris flow control projects in southwest  
546 mountains areas of China, *J. Chengdu Univ. Technol. (Science Technol. Ed.)*, 40, 50–58, <https://doi.org/10.3969/j.issn.1671->  
547 [9727.2013.01.008](https://doi.org/10.3969/j.issn.1671-9727.2013.01.008), 2013.
- 548 Chen, X., Li, Z., Cui, P., and Liu, X.: Estimation of soil erosion caused by the 5.12 Wenchuan Earthquake, *J. Mt. Sci.*, 27,  
549 122–127, 2009.
- 550 [Chen, X., Cui, P., You, Y., Chen, J., and Li, D.: Engineering measures for debris flow hazard mitigation in the Wenchuan](https://doi.org/10.1016/j.enggeo.2014.10.002)  
551 [earthquake area, \*Eng. Geol.\*, 194, 73–85, <https://doi.org/10.1016/j.enggeo.2014.10.002>, 2015.](https://doi.org/10.1016/j.enggeo.2014.10.002)
- 552 [Chen, Y., Li, J., Jiao, J., Wang, N., Bai, L., Chen, T., Zhao, C., Zhang, Z., Xu, Q., and Han, J.: Modeling the impacts of](https://doi.org/10.1016/j.ejrh.2022.101290)  
553 [fully-filled check dams on flood processes using CAESAR-lisflood model in the Shejiagou catchment of the Loess Plateau,](https://doi.org/10.1016/j.ejrh.2022.101290)  
554 [China, \*J. Hydrol. Reg. Stud.\*, 45, 101290, <https://doi.org/10.1016/j.ejrh.2022.101290>, 2023.](https://doi.org/10.1016/j.ejrh.2022.101290)
- 555 Cong, K., Li, R., and Bi, Y.: Benefit evaluation of debris flow control engineering based on the FLO-2D model, *Northwest*  
556 *Geol.*, 52, <https://doi.org/10.19751/j.cnki.61-1149/p.2019.03.019>, 2019.
- 557 Couclelis, H.: From cellular automata to urban models: new principles for model development and implementation, *Environ.*  
558 *Plan. B Plan. Des.*, 24, 165–174, <https://doi.org/10.1068/b240165>, 1997.
- 559 Coulthard, T. J. and Skinner, C. J.: The sensitivity of landscape evolution models to spatial and temporal rainfall resolution,  
560 *Earth Surf. Dyn.*, 4, 757–771, <https://doi.org/10.5194/esurf-4-757-2016>, 2016.
- 561 Coulthard, T. J. and ~~Wiel, Van De~~ ~~Wiel, J., M.-J.~~: Modelling long term basin scale sediment connectivity, driven by spatial  
562 land use changes, *Geomorphology*, 277, 265–281, <https://doi.org/10.1016/j.geomorph.2016.05.027>, 2017.
- 563 Coulthard, T. J., Macklin, M. G., and Kirkby, M. J.: A cellular model of Holocene upland river basin and alluvial fan  
564 evolution, *Earth Surf. Process. Landforms*, 27, 269–288, <https://doi.org/10.1002/esp.318>, 2002.
- 565 Coulthard, T. J., Hancock, G. R., and Lowry, J. B. C.: Modelling soil erosion with a downscaled landscape evolution model,  
566 *Earth Surf. Process. Landforms*, 37, 1046–1055, <https://doi.org/10.1002/esp.3226>, 2012a.
- 567 Coulthard, T. J., Ramirez, J., Fowler, H. J., and Glenis, V.: Using the UKCP09 probabilistic scenarios to model the amplified  
568 impact of climate change on drainage basin sediment yield, *Hydrol. Earth Syst. Sci.*, 16, 4401–4416,  
569 <https://doi.org/10.5194/hess-16-4401-2012>, 2012b.
- 570 Coulthard, T. J., Neal, J. C., Bates, P. D., Ramirez, J., de Almeida, G. A. M., and Hancock, G. R.: Integrating the  
571 LISFLOOD-FP 2D hydrodynamic model with the CAESAR model: Implications for modelling landscape evolution, *Earth*  
572 *Surf. Process. Landforms*, 38, 1897–1906, <https://doi.org/10.1002/esp.3478>, 2013.
- 573 Cui, P. and Lin, Y.: Debris-Flow Treatment: The Integration of Botanical and Geotechnical Methods, *J. Resour. Ecol.*, 4,  
574 097–104, <https://doi.org/10.5814/j.issn.1674-764x.2013.02.001>, 2013.
- 575 Cui, P., Zhou, G. G. D., Zhu, X. H., and Zhang, J. Q.: Scale amplification of natural debris flows caused by cascading  
576 landslide dam failures, *Geomorphology*, 182, 173–189, <https://doi.org/10.1016/j.geomorph.2012.11.009>, 2013.



577 ~~East, A. E., D'Agostino, V., and Sankey, J. B.: Geomorphic and Sedimentary Effects of Modern Climate Change: Current and~~  
578 ~~Anticipated Future Conditions~~ Lenzi, M. A.: Bedload transport in the Western United States, Rev. Geophys., 58  
579 instrumented  
580 catchment of the Rio Cordon. Part II: Analysis of the bedload rate, Catena, 36, 191–204,  
581 https://doi.org/10.1029/2019RG000692, 2020 1016/S0341-8162(99)00017-X, 1999.

581 Einstein, H. A.: The Bed-Load Function for Sediment Transportation in Open Channel Flows, 1950.

582 Fan, X., Yang, F., Siva Subramanian, S., Xu, Q., Feng, Z., Mavrouli, O., Peng, M., Ouyang, C., Jansen, J. D., and Huang, R.:  
583 Prediction of a multi-hazard chain by an integrated numerical simulation approach: the Baige landslide, Jinsha River, China,  
584 Landslides, 17, 147–164, <https://doi.org/10.1007/s10346-019-01313-5>, 2020.

585 Feng, W., He, S., Liu, Z., Yi, X., and Bai, H.: Features of Debris Flows and Their Engineering Control Effects at Xinping  
586 Gully of Pingwu County, J. Eng. Geol., 25, <https://doi.org/10.13544/j.cnki.jeg.2017.03.027>, 2017.

587 Forbes, K. and Broadhead, J.: Forests and landslides: the role of trees and forests in the prevention of landslides and  
588 rehabilitation of landslide-affected areas in Asia, FAO, 14–18 pp., 2013.

589 Gioia, D. and Schiattarella, M.: Modeling Short-Term Landscape Modification and Sedimentary Budget Induced by Dam  
590 Removal: Insights from LEM Application, Appl. Sci., 10, 7697, <https://doi.org/10.3390/app10217697>, 2020.

591 Goldberg, D. E.: Genetic Algorithms in Search, Optimization, and Machine Learning, Addison-Wesley Longman Publishing  
592 Co., Inc., 372 pp., <https://doi.org/10.1007/BF01920603>, 1989.

593 Gorum, T., Fan, X., van Westen, C. J., Huang, R. Q., Xu, Q., Tang, C., and Wang, G.: Distribution pattern of earthquake-  
594 induced landslides triggered by the 12 May 2008 Wenchuan earthquake, Geomorphology, 133, 152–167,  
595 <https://doi.org/10.1016/j.geomorph.2010.12.030>, 2011.

596 Guo, Q., Xiao, J., and Guan, X.: The characteristics of debris flow activities and its optimal timing for the control in Shikan  
597 River Basin Pingwu Country, Chinese J. Geol. Hazard Control, 29, [https://doi.org/10.16031/j.cnki.issn.1003-8035.2018.](https://doi.org/10.16031/j.cnki.issn.1003-8035.2018.03.05)  
598 03.05, 2018.

599 Hancock, G. R., Verdon-Kidd, D., and Lowry, J. B. C.: Soil erosion predictions from a landscape evolution model – An  
600 assessment of a post-mining landform using spatial climate change analogues, Sci. Total Environ., 601–602, 109–121,  
601 <https://doi.org/10.1016/j.scitotenv.2017.04.038>, 2017.

602 ~~Hassanli, A. M. and Beecham, S.: Criteria for optimizing check dam location and maintenance requirements, Check Dams,~~  
603 ~~Morphol. Adjust. Eros. Control Torrential Streams, 11–31, 2013.~~

604 He, J., Zhang, L., Fan, R., Zhou, S., Luo, H., and Peng, D.: Evaluating effectiveness of mitigation measures for large debris  
605 flows in Wenchuan, China, Landslides, 19, 913–928, <https://doi.org/10.1007/s10346-021-01809-z>, 2022.

606 Huang, R.: Geohazard assessment of the Wenchuan earthquake, Science Press, Beijing, 944 pp., 2009.

607 Huang, R. and Fan, X.: The landslide story, Nat. Geosci., 6, 325–326, <https://doi.org/10.1038/ngeo1806>, 2013.

608 J.B.C. Lowry, M. Narayan, G.R. Hancock, ~~K.G. Evans,~~ and K.G. Evans: Understanding post-mining landforms: Utilising pre-  
609 mine geomorphology to improve rehabilitation outcomes, Geomorphology, 328, 93–107,  
610 <https://doi.org/10.1016/j.geomorph.2018.11.027>, 2019.

611 Lan, H., Wang, D., He, S., Fang, Y., Chen, W., Zhao, P., and Qi, Y.: Experimental study on the effects of tree planting on  
612 slope stability, Landslides, 17, 1021–1035, <https://doi.org/10.1007/s10346-020-01348-z>, 2020.

613 Lee, T. and Jeong, C.: Nonparametric statistical temporal downscaling of daily precipitation to hourly precipitation and  
614 implications for climate change scenarios, J. Hydrol., 510, 182–196, <https://doi.org/10.1016/j.jhydrol.2013.12.027>, 2014.

615 Li, C., Wang, M., and Liu, K.: A decadal evolution of landslides and debris flows after the Wenchuan earthquake,  
616 Geomorphology, 323, 1–12, <https://doi.org/10.1016/j.geomorph.2018.09.010>, 2018.

617 Li, C., Wang, M., Liu, K., and Coulthard, T. J.: Landscape evolution of the Wenchuan earthquake-stricken area in response  
618 to future climate change, J. Hydrol., 590, 125244, <https://doi.org/10.1016/j.jhydrol.2020.125244>, 2020.

619 [Luan, J., Miao, P., Tian, X., Li, X., Ma, N., Xu, Z., Wang, H., and Zhang, Y.: Separating the impact of check dams on runoff](#)  
620 [from climate and vegetation changes, \*J. Hydrol.\*, 614, 128565, <https://doi.org/10.1016/j.jhydrol.2022.128565>, 2022.](#)

621 Marchi, L., Comiti, F., Crema, S., and Cavalli, M.: Channel control works and sediment connectivity in the European Alps,  
622 *Sci. Total Environ.*, 668, 389–399, <https://doi.org/10.1016/j.scitotenv.2019.02.416>, 2019.

623 Mickovski, S. B., Bengough, A. G., Bransby, M. F., Davies, M. C. R., Hallett, P. D., and Sonnenberg, R.: Material stiffness,  
624 branching pattern and soil matric potential affect the pullout resistance of model root systems, *Eur. J. Soil Sci.*, 58, 1471–  
625 1481, <https://doi.org/10.1111/j.1365-2389.2007.00953.x>, 2007.

626 Poepl, R. E., Coulthard, T., Keesstra, S. D., and Keiler, M.: Modeling the impact of dam removal on channel evolution and  
627 sediment delivery in a multiple dam setting, *Int. J. Sediment Res.*, 34, 537–549, <https://doi.org/10.1016/j.ijsrc.2019.06.001>,  
628 2019.

629 Ramirez, J. A., Zischg, A. P., Schürmann, S., Zimmermann, M., Weingartner, R., Coulthard, T., and Keiler, M.: Modeling  
630 the geomorphic response to early river engineering works using CAESAR-Lisflood, *Anthropocene*, 32,  
631 <https://doi.org/10.1016/j.ancene.2020.100266>, 2020.

632 Ramirez, J. A., Mertin, M., Peleg, N., Horton, P., Skinner, C., Zimmermann, M., and Keiler, M.: Modelling the long-term  
633 geomorphic response to check dam failures in an alpine channel with CAESAR-Lisflood, *Int. J. Sediment Res.*, 37, 687–700,  
634 <https://doi.org/10.1016/j.ijsrc.2022.04.005>, 2022.

635 Reichenbach, P., Busca, C., Mondini, A. C., and Rossi, M.: The Influence of Land Use Change on Landslide Susceptibility  
636 Zonation: The Briga Catchment Test Site (Messina, Italy), *Environ. Manage.*, 54, 1372–1384,  
637 <https://doi.org/10.1007/s00267-014-0357-0>, 2014.

638 Saynor, M. J., Lowry, J. B. C., and Boyden, J. M.: Assessment of rip lines using CAESAR-Lisflood on a trial landform at the  
639 Ranger Uranium Mine, *L. Degrad. Dev.*, 30, 504–514, <https://doi.org/10.1002/ldr.3242>, 2019.

640 Skinner, C. J., Coulthard, T. J., Schwanghart, W., Van De Wiel, M. J., and Hancock, G.: Global sensitivity analysis of  
641 parameter uncertainty in landscape evolution models, *Geosci. Model Dev.*, 11, 4873–4888, [https://doi.org/10.5194/gmd-11-](https://doi.org/10.5194/gmd-11-4873-2018)  
642 [4873-2018](https://doi.org/10.5194/gmd-11-4873-2018), [2018a](#).

643 [Skinner, C. J., Coulthard, T. J., Schwanghart, W., Van De Wiel, M. J., and Hancock, G.: Global sensitivity analysis of](#)  
644 [parameter uncertainty in landscape evolution models, \*Geosci. Model Dev.\*, 11, 4873–4888, \[https://doi.org/10.5194/gmd-11-\]\(https://doi.org/10.5194/gmd-11-4873-2018\)](#)  
645 [4873-2018](#), [2018b](#).

646 Slingerland, N., Beier, N., and Wilson, G.: Stress testing geomorphic and traditional tailings dam designs for closure using a  
647 landscape evolution model, in: *Proceedings of the 13th International Conference on Mine Closure*, 1533–1544,  
648 [https://doi.org/10.36487/ACG\\_rep/1915\\_120\\_Slingerland](https://doi.org/10.36487/ACG_rep/1915_120_Slingerland), 2019.

649 Stokes, A., Douglas, G. B., Fourcaud, T., Giadrossich, F., Gillies, C., Hubble, T., Kim, J. H., Loades, K. W., Mao, Z.,  
650 McIvor, I. R., Mickovski, S. B., Mitchell, S., Osman, N., Phillips, C., Poesen, J., Polster, D., Preti, F., Raymond, P., Rey, F.,  
651 Schwarz, M., and Walker, L. R.: Ecological mitigation of hillslope instability: Ten key issues facing researchers and  
652 practitioners, *Plant Soil*, 377, 1–23, <https://doi.org/10.1007/s11104-014-2044-6>, 2014.

653 Thomson, H. and Chandler, L.: Tailings storage facility landform evolution modelling, in: *Proceedings of the 13th*  
654 *International Conference on Mine Closure*, 385–396, [https://doi.org/10.36487/ACG\\_rep/1915\\_31\\_Thomson](https://doi.org/10.36487/ACG_rep/1915_31_Thomson), 2019.

655 Wang, M., Yang, W., Shi, P., Xu, C., and Liu, L.: Diagnosis of vegetation recovery in mountainous regions after the  
656 wenchuan earthquake, *IEEE J. Sel. Top. Appl. Earth Obs. Remote Sens.*, 7, 3029–3037,  
657 <https://doi.org/10.1109/JSTARS.2014.2327794>, 2014a.

658 Wang, M., Liu, M., Yang, S., and Shi, P.: Incorporating Triggering and Environmental Factors in the Analysis of  
659 Earthquake-Induced Landslide Hazards, *Int. J. Disaster Risk Sci.*, 5, 125–135, <https://doi.org/10.1007/s13753-014-0020-7>,  
660 2014b.

661 Wang, N., Han, B., Pang, Q., and Yu, Z.: post-evaluation model on effectiveness of debris flow control, *J. Eng. Geol.*, 23,  
662 219–226, <https://doi.org/10.13544/j.cnki.jeg.2015.02.005>, 2015.

663 Van De Wiel, M. J., Coulthard, T. J., Macklin, M. G., and Lewin, J.: Embedding reach-scale fluvial dynamics within the  
664 CAESAR cellular automaton landscape evolution model, *Geomorphology*, 90, 283–301,  
665 <https://doi.org/10.1016/j.geomorph.2006.10.024>, 2007.

666 Wilcock, P. R., Asce, M., and Crowe, J. C.: Surface-based Transport Model for Mixed-Size Sediment Surface-based  
667 Transport Model for Mixed-Size Sediment, 9429, [https://doi.org/10.1061/\(ASCE\)0733-9429\(2003\)129](https://doi.org/10.1061/(ASCE)0733-9429(2003)129), 2003.

668 Xie, J., Wang, M., Liu, K., and Coulthard, T. J.: Modeling sediment movement and channel response to rainfall variability  
669 after a major earthquake, *Geomorphology*, 320, 18–32, <https://doi.org/10.1016/j.geomorph.2018.07.022>, 2018.

670 [Xie, J., Coulthard, T. J., and McLelland, S. J.: Modelling the impact of seismic triggered landslide location on basin  
671 sediment yield, dynamics and connectivity, \*Geomorphology\*, 398, 108029, <https://doi.org/10.1016/j.geomorph.2021.108029>,  
672 2022a.](https://doi.org/10.1016/j.geomorph.2021.108029)

673 [Xie, J., Coulthard, T. J., Wang, M., and Wu, J.: Tracing seismic landslide-derived sediment dynamics in response to climate  
674 change, \*Catena\*, 217, 106495, <https://doi.org/10.1016/j.catena.2022.106495>, 2022b.](https://doi.org/10.1016/j.catena.2022.106495)

675 Xu, C., Xu, X., Yao, X., and Dai, F.: Three (nearly) complete inventories of landslides triggered by the May 12, 2008  
676 Wenchuan Mw 7.9 earthquake of China and their spatial distribution statistical analysis, *Landslides*, 11, 441–461,  
677 <https://doi.org/10.1007/s10346-013-0404-6>, 2014.

678 [Yager, E. M., Turowski, J. M., Rickenman, D., and McArdeell, B. W.: Sediment supply, grain protrusion, and bedload  
679 transport in mountain streams, \*Geophys. Res. Lett.\*, 39, 1–5, <https://doi.org/10.1029/2012GL051654>, 2012.](https://doi.org/10.1029/2012GL051654)

680 Yang, Z., Duan, X., Huang, J., Dong, Y., Zhang, X., Liu, J., and Yang, C.: Tracking long-term cascade check dam siltation:  
681 implications for debris flow control and landslide stability, *Landslides*, 18, 3923–3935, [https://doi.org/10.1007/s10346-021-  
01755-w](https://doi.org/10.1007/s10346-021-<br/>682 01755-w), 2021.

683 Yeh, A. G. O. and Li, X.: Errors and uncertainties in urban cellular automata, *Comput. Environ. Urban Syst.*, 30, 10–28,  
684 <https://doi.org/10.1016/j.compenvurbnsys.2004.05.007>, 2006.

685 Yu, B., Yang, Y., Su, Y., Huang, W., and Wang, G.: Research on the giant debris flow hazards in Zhouqu County, Gansu  
686 Province on August 7, 2010, *J. Eng. Geol.*, 18, 437–444, <https://doi.org/10.3969/j.issn.1004-9665.2010.04.001>, 2010.

687 Zhang, L. and Liang, K.: Research on economic benefit evaluation of the prevention and cure project for debris flow,  
688 *Chinese J. Geol. Hazard Control*, 16, 48–53, <https://doi.org/10.3969/j.issn.1003-8035.2005.03.011>, 2005.

689 Zhang, X., Wang, M., Liu, K., Xie, J., and Xu, H.: Using NDVI time series to diagnose vegetation recovery after major  
690 earthquake based on dynamic time warping and lower bound distance, *Ecol. Indic.*, 94, 52–61,  
691 <https://doi.org/10.1016/j.ecolind.2018.06.026>, 2018.

692 Zhou, H., Chen, N., Lu, Y., and Li, B.: Control Effectiveness of Check Dams in Debris Flow Gully: A Case of Huashiban  
693 Gully in Earthquake Worst-stricken Area, Beichuan County, *J. Mt. Sci.*, 30, 347–354, [https://doi.org/10.3969/j.issn.1008-  
2786.2012.03.015](https://doi.org/10.3969/j.issn.1008-<br/>694 2786.2012.03.015), 2012.

695